R/V ALKOR Cruise Report AL447

Controls on methane seepage in the Baltic Sea

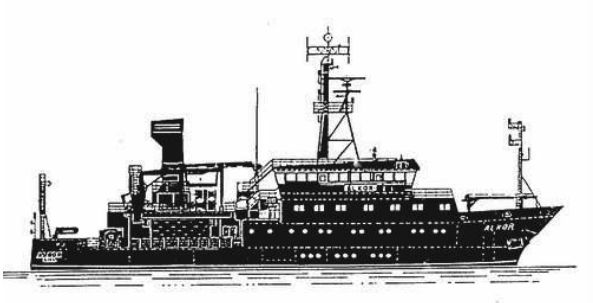

20th Oct. – 04th Nov., 2014

Kiel-Kiel (Germany)

Jens Schneider von Deimling

and cruise participants

GEOMAR Helmholtz Centre for Ocean Research Kiel

Wischhofstr. 1-3

24148 Kiel, Germany

Cruise Report AL447 published April 2015

DOI: 10.3289/CR_AL447

Table of Contents

Introduction

After water vapor and carbon dioxide (CO_2), methane (CH_4) is the most relevant greenhouse gas on Earth, contributing for about 20% to radiative forcing by well-mixed greenhouse gases on a century timescale (IPCC, 2013). Natural methane release from the seafloor by seep processes is observed virtually on all continental margins (Judd and Hovland, 2007), and its significance for the atmospheric methane budget and global warming is still under debate (IPCC, 2013). Estimates suggest marine seeps may contribute 10–30 Tg yr^{-1} (Kvenvolden et al., 2001) out of an global geological emissions of 30–45 Tg yr^{-1} (Etiope and Klusman, 2002).

Due to their high organic matter content, continental slope and marginal sea sediments have a huge CH_4 generation potential by biogenic or thermogenic processes (Judd and Hovland, 2007; Reeburgh, 2007). Consequently, methane release from the seabed by seepage processes is observed virtually on all continental margins (Judd and Hovland, 2007).

In the North Sea biogenic and thermogenic methane seepage are common phenomena, especially along its central buried geological graben (Figure 1), and have been investigated since decades (Hovland and Sommerville, 1985; Judd and Hovland 2007). Shallow gas hosted in the sediments can enter the water column by diffusion, fluid flow, and gas bubble release. Gas bubble seepage is especially efficient in by-passing the microbial filter of the shallow seabed and free gas release was occasionally observed in echosounder data in the North Sea (Judd et al., 1997; Hovland and Sommerville, 1985; Schroot et al., 2005; Niemann et al., 2005; Schneider von Deimling et al., 2010, 2011). However, direct impact from gas seepage on atmospheric sea-air flux of methane especially in the Central and Northern North Sea during summer was found to be low (Rehder et al. 1998). The reasons are that quick methane gas bubble dissolution predominantly takes place at depth, and diapycnal mixing of seepage-mediated methane is strongly hampered across the intense thermocline (Schneider von Deimling et al., 2011) persisting throughout summer and fall (Figure 1) in the North Sea (Holt and Umlauf, 2008).

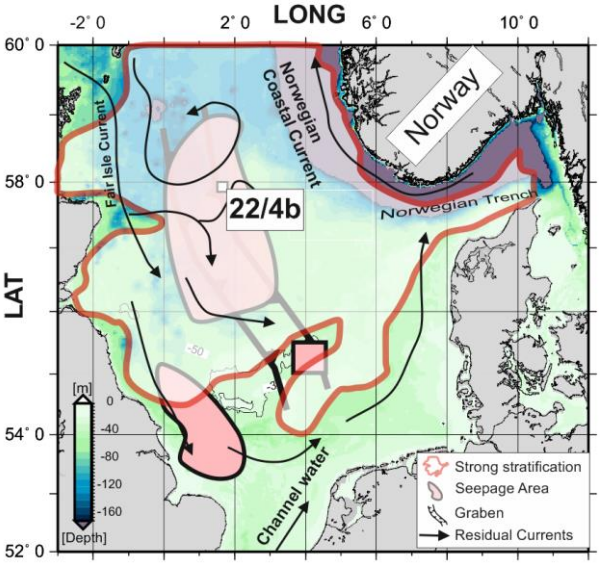

Figure 1: North Sea bathymetry (http://www.gebco.net) with schematic hydrographic information of the main flow pattern adapted from Turrell et al. (1992). Three gas seepage regions (orange polygons) surrounding the study area 22/4b were compiled from various sources (Judd et al., 1997; Judd 2001; Schroot et al., 2005). Shaded polygon with brown border shows the spatial extent of strong stratification (ΔT~6K) between surface and bottom water in the North Sea modeled for June–August after Holt and Umlauf (2008). Figure is adapted from Schneider von Deimling (2009).

The proposed research cruise shall cover methodological and research goals under the framework of the European joint research projects SUGAR II and ECO2. One goal of the cruise is to test new acoustic remote sensing tools for the evaluation of gas seep sites in the North Sea. In addition external controls on seepage are evaluated to better understand triggering mechanisms and to constrain the fate of the gases. The question if currents and tides have a significant impact on bubble emission characteristics and gas plume dynamics shall be

addressed. Supporting geochemical records of dissolved methane concentration and CH_4 gradients in the air shall be recorded to improve the understanding of the fate of gaseous and dissolved seepage methane, respective gas bubble dissolution, and potential transfer to the atmosphere.

This research cruise got scheduled for late fall and given a very stormy period the work was limited to protected areas. We decided to sample the natural seepage sites in the Eckernförde Bay and the bubbling reefs off Læsø instead of the remote offshore seepage sites in the North Sea. Both sites are known for their consistent methane seepage activity of thermogenic (Jensen et al., 1992) and biogenic origin (Whiticar, 1981), respectively. Both research areas offer the possibility to sail towards the pristine research areas in the North Sea within a reasonable steaming time, once the weather would have improved. Apart from the natural gas seepage sites, an artificial gas release lander was brought to generate a calibrated and video controlled in situ gas flux. This allows for calibrated acoustic measurements and quantitative gas flux estimates coupled with multibeam for spatial extrapolations.

Narrative of the Cruise

Severe weather in the North Sea prohibited to reach the primary areas of interest, that would have required at least three days of calm weather in a row to complete steaming to, sampling of, and getting away from the offshore seepage areas in the North Sea. Therefore we decided to stay close to the Kiel Channel and the Skagerrak, respectively, to take any chance to quickly steam into the North Sea if possible. A period with waves between 3 to 6 m height and strong westerly winds persisted throughout the time of the cruise and only an intermittent calmer period of a maximum of 20 hours occurred in the forecasts for the North Sea. Therefore a well prepared alternate research program was conducted in the Baltic Sea (Figure 10).

19.10 On the first day equipment was mobilized including installation of a new generation multibeam echosounder together with satellite GPS correction support (FUGRO) on R/V ALKOR. This required the adaption of the moonpool plate beforehand, peer-site measurement of position offsets (transducer-antennas-MRU) as well as setup of IT infrastructure to handle the excessive water column imaging data streams. Loading of the research vessel and installation of the multibeam and ADCP was successfully completed in time and the cruise could begin on Monday the **20th of October**. First the EK60 singlebeam system had to be calibrated with copper spheres for sonar target strength measurements. This task was performed in the well-protected Kiel Fjord. In the evening, R/V ALKOR took off to the outer Kiel Fjord to perform the first motion sensor calibration and multibeam measurements until **21st of October**. The motion sensor calibration did not achieve specification and required re-sailing “eights” for several hours. After acquiring a reasonable state of calibration we started to sail towards Eckernförde Bay. Between the 21st and **the 22nd** the known pockmarks close to the shallow “Mittelgrund” area were surveyed with the new high resolution multibeam echosounder allowing for inspection of the water column scatterers with a hitherto unprecedented resolution. A significant water level change was predicted to occur and therefore repeated surveys for free gas bubble release detection were started. Unfortunately, this task had to be abandoned in the morning of Tuesday **23rd** due to a medical issue. One crew member had to be transferred to the hospital of Kiel, nevertheless R/V ALKOR could leave the harbor in the evening again with all crew members back on board.

The weather situation in the North Sea remained stormy. Repeated sampling in Eckernförde Bay was continued on the **24th and 25th** to evaluate whether gas ebullitions are linked to water level changes. This included two in situ lander deployments covering more than 30 hours to monitor gas ebullition over varying water levels and pressure conditions. Other equipment was tested in the hope of later deployment in the North Sea. We successfully deployed the Bubble Box mounted onto the OFOS frame and captured naturally released gas bubbles. After finishing a comprehensive flare imaging survey R/V ALKOR steamed towards the Kattegat with arrival 18 hours later on the **27th of October**. The area north of the island Læsø belongs to a protected natural reservat known for its "bubbling reefs". In co-operation with our Danish colleagues we were asked to first survey the hitherto un-surveyed areas north of Læsø with the capabilities of our newly installed multibeam echosounder. However, the motion sensor performance worsened. A port call was necessary in the harbor of Frederikshavn on the evening of the 27th for re-measurement of the static offsets between the antennas and the multibeam using a land-based reference station. Moreover, the ship's oar was inspected by divers due to some problems identified during the cruise so far. After successful correction for an offset error R/V ALKOR left the harbor in the morning of the **28th** again. Subsequently, the motion sensor unit performed fine and successfully calibrated. Work could be continued north of Læsø. After identification of one consistent gas releasing seep spot we further decided to deploy the tripod gas monitoring lander for 20 hours. On the **29th** we got informed about potential contamination by legionella bacteria via the freshwater tanks of ALKOR. Each member of the scientific crew had to be interviewed if they would prefer to disembark the vessel, but everybody declined. However the Danish observer, who should have entered the vessel to support the surveying within the restricted 3 nautical miles Danish coastal zone including the protected bubbling reefs, declined participation under the prevailing conditions. Therefore the research plan had to be changed again to surveying outside the 3 nautical mile zone. The weather situation in the North Sea did not improve and acquisition of a valuable dataset at the Blowout site turned unrealistic within the remaining time of the cruise. Another severe southwesterly wind was predicted, likely causing significant water level low in Eckernförde Bay. To verify our previous results with extraordinary high methane ebullition triggered by wind driven water level lows, we decided to steam back to Eckernförde in the evening of the **31st**. On the **1st** and **2nd of November** work off Eckernförde including flare imaging and water column methane analyses was continued and the GasQuant II lander got deployed for 24 hours. For the gas elevator lander deployment a sandy area was necessary for a successful deployment on the seabed on the **3rd** of November. Such a site was identified off Schönberg (East of the outer Kiel Fjord) and confirmed by a grab sample. The artificial gas release system was working perfectly fine and succeeding acoustic measurements will allow for a later calibration of acoustic gas flux determination. Subsequently we further mapped the seabed for dumped munition to meet a cooperation agreement made prior to AL447 until the end of the cruise in the morning of the **4th** of November.

Participants

Table 1 Scientific crew participants during AL447.

Name	Discipline	Institution
Dr. Jens Schneider v.D.	Chief scientist, multibeam	GEOMAR
Dr. Ilia Ostrovsky	Senior scientist, EK60	University Haifa (Israel)
Dr. Helge Niemann	Senior scientist, CH_4 analysis	University Basel (Switzerland)
Dr. Philipp Held	Senior scientist, Innomar subbottom	GEOMAR
Asmus Petersen	Technician	GEOMAR
Sergiy Cherednichenko	Technician	GEOMAR
Peter Urban	PHD student, Lander GasQuant II	GEOMAR
Dominik Richner	Master student	University Basel
Jasper Hoffmann	Student geophysics	GEOMAR
Arne Lohrberg	Student geophysics	GEOMAR
Tina Kunde	Student geomatics	HCU Hamburg

Figure 2: Group picture of scientific crew of AL447.

Methodology and Preliminary Results

Acoustic and Optic Gas Seepage Observations

Methodology

Multibeam EM2040c

For the first time a fifth generation KONGSBERG EM2040c shallow water multibeam system was installed on R/V ALKOR. The broadband 200–400 kHz transducer was mounted on a special moonpool-pole flange (Figure 3). The shape of the transducer is circular, but the TX/RX array is internally arranged in a Mills-Cross configuration where the EM2040C represents the more compact and smaller version of the EM2040 series with a 130° opening angle. The system fully supports near field focusing both on transmit and receive as well as water column imaging and includes a "3D scanning" pitch steering function that is ideally suited for gas bubble tracking as suggested in Schneider von Deimling and Papenberg (2012). Keel sound velocity were measured online next to the sonar head with an AML mini keel sound velocity probe and respective vertical profiles were taken with the shipboard CTD system.

Figure 3: Mobile installation of the EM2040c multibeam transducer (red) and the 300 kHz RDI ADCP (yellow) in the moonpool; 19.10.2014, R/V ALKOR

For accurate ship positioning and motion compensation a pair of F180 Codaoctopus GPS antennas were installed on the top deck and connected with their wetpod inertial motion unit in the moonpool (IMU). The F180 IMU was further supported by an extra antenna receiving commercial satellite DGPS correction data (provided by Fugro). The GPS reference ellipsoid was set to WGS84. Positions and heading (10 Hz) as well as roll, pitch and heave and pulse per second (PPS) timing signals were sent to the multibeam system.

Water column imaging data were recorded in a way not to lose the spatial coherence of potential rising and current-deflected gas bubble streams. The pulse length was set constant allowing for later comparison of echo scattering strengths. Bathymetry (.all) and water column data (.wcd) were visualized with SIS and streamed over a gigabit-ethernet controller to a performance RAID 10 NAS server for safe online storage, post-processing, and later review.

Frequent CTD casts were acquired in all survey areas to account for the very high tempo-spatial variations of sound velocity in the Baltic Sea. 'Best fit' profiles were manually selected in post-processing to minimize sound refraction errors.

Multibeam Data Processing

The raw .all data were imported with MBSystem version 5.4 for review of navigation and motion data, re-calculation of bathymetry after sound velocity and water-level correction, filtering, editing, and visualization. Threshold filtering was realized with an area-based filter in MBSystem to remove the soundings with standard deviations exceeding factor two to three.

In areas where gas seep bubbles occurred the data were evaluated in 3D to manually mitigate bottom detection mismatches. NETCDF grids were created using a median filter with a grid size

according to the local water depth and with respect to the array beamwidth of the EM2040c. Water column imaging data (.wcd) were left unprocessed and got visualized in Fledermaus-FMMidwater, snippet sidescan in FMGeocoder.

Singlebeam EK60 System and Elevator Lander

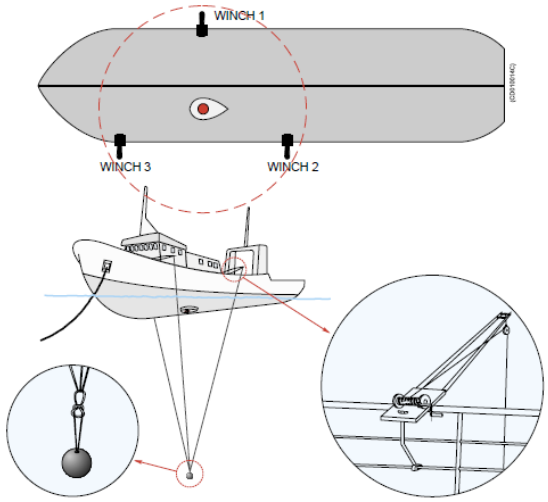

Figure 4: Schematic drawing of lowering the copper sphere into the sound beam.

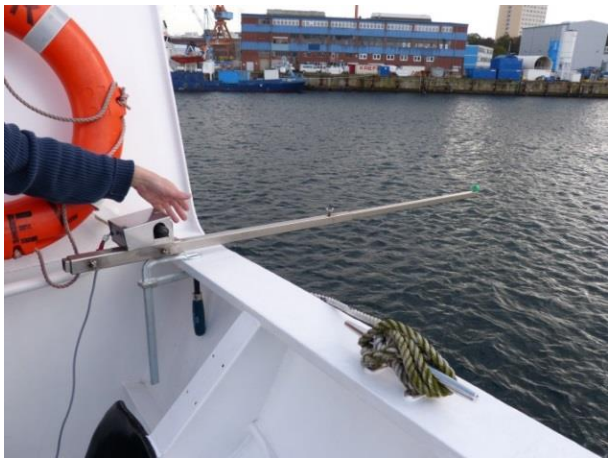

Figure 5: Device on R/V ALKOR for controlling the position of the sphere, similar to a fishing rod.

In order to maintain the accuracy of the Simrad EK60 required for scientific applications, it must be calibrated. During calibration a reference target copper sphere with known target strength was lowered into the sound beam and the measured target strength was compared with the known target strength (Figure 6).

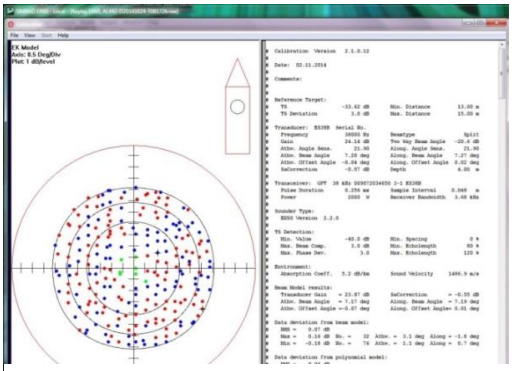

Figure 6: Rigging the vessel for sphere calibration and lowering the copper sphere into the sonar beam.

Each frequency was calibrated individually with a respective copper sphere at given pulse duration. Calibration was done at a range of about 9-11 m.

INNOMAR Parametric Subbottom Sounder

The seismic profiles were recorded with a parametric subbottom profiler of type Innomar SES-2000® medium. This device is hull-mounted on R/V ALKOR. It transmits two high frequencies at high sound pressure. These two sound waves interact in the water column, generating harmonics. The SES-2000® medium records one of the primary frequencies of about 100 kHz and the difference frequency of the primaries. The advantage of parametric echosounders is that the difference frequency, the so-called secondary, has a similar beam width as the primaries. Therefore, it is possible to generate a low frequency with narrow beam width and a small transducer. The secondary frequency is adjustable and was set to 4 kHz during the surveys in the Eckernförde Bay and to 5 kHz during the surveys at Læsø. The system has a vertical resolution of 6 cm and its accuracy depends on the frequency and water depth, e.g. 100/10 kHz: 2/4 cm + 0.02% of the water depth (Wunderlich and Müller, 2003). The soundbeam is corrected for heave, roll and pitch movements of the vessel.

After recording, the data were converted into the segy-format and to be further processed with the freely available Seismic Unix-toolbox.

GasQuant Imaginex

The GasQuant II system (Figure 7) is a multibeam based lander system for monitoring of free gas release (bubbles). It is currently being further developed by GEOMAR to become the successor of the GasQuant I system (Greinert, 2008) and is built for autonomous operation on the seafloor. In contrary to its predecessor, it is a light weight and low-power device that can be deployed by small vessels or ROVs.

Figure 7: GasQuant II system before the first deployment

The used sonar device is an Imagenex Delta T 837b multibeam system that features a low power consumption of only 5 watt by covering a range of up to 100 m. The multibeam is operated from a minicomputer and powered by a 2000 kWh lithium ion battery. A custom written C++ program on the minicomputer directly controls the Imagenex by requesting every ping individually and then saves the received data to an internal hard-drive as Imagenex .837 files. With this program it is possible to change the setup for every individual ping, including pulse length, recording range, and ping rate. The Imagenex reserves 500 sample values for the return of each ping, therefore, setting the range of the system directly affects the range resolution of the output data.

The system can be deployed in two different ways: Forward looking and upward looking. In forward looking mode, the multibeam swath is steered horizontally above the sea floor. The receive signal therefore corresponds to a horizontal slice through the water column. In this mode the system has the largest seafloor coverage and is therefore prone for area based monitoring. However when single bubble releases are dominant in an area it is difficult in the forward looking mode to distinguish bubble reflections from fish or other noise signals. In the upward looking mode single bubbles can be easily detected and the bubble rising velocities can be determined but the coverage area is reduced to a narrow slice.

The Key Features of the entire system are:

Table 2: GasQuant II system specifications

Weight (entire system)	ca. 40 kg
Range	50-100 m
Swath opening angle	120°
Base frequency	260 kHz
Operation time	up to 3 days
Depth rating	4000 m

During cruise AL447 the prototype of GasQuant II has been deployed to investigate the possible temporal variability of the marine gas emission at known seeps, but also to test the prototype system. The prototype is still missing an integrated compass and attitude sensor. Due to these shortcomings precise georeferencing of the sonar data is not yet available.

Bubble Box / OFOS / Elevator Lander

For the assessment of bubble size distribution, bubble rise velocity, and resulting gas fluxes, a bubble imaging box (BBOX) was constructed at GEOMAR in the framework of SUGAR II (Figure 8). The BBOX can be used open top or with a closing lid to either allow undisturbed vertical flow-though, or precise flux measurements into predefined capture volumes. The front and sidewalls are made of transparent acrylic glass for ROV video observation, while the backwall is made of a white acryl glass acting as a light diffuser for the LED backlid illumination.

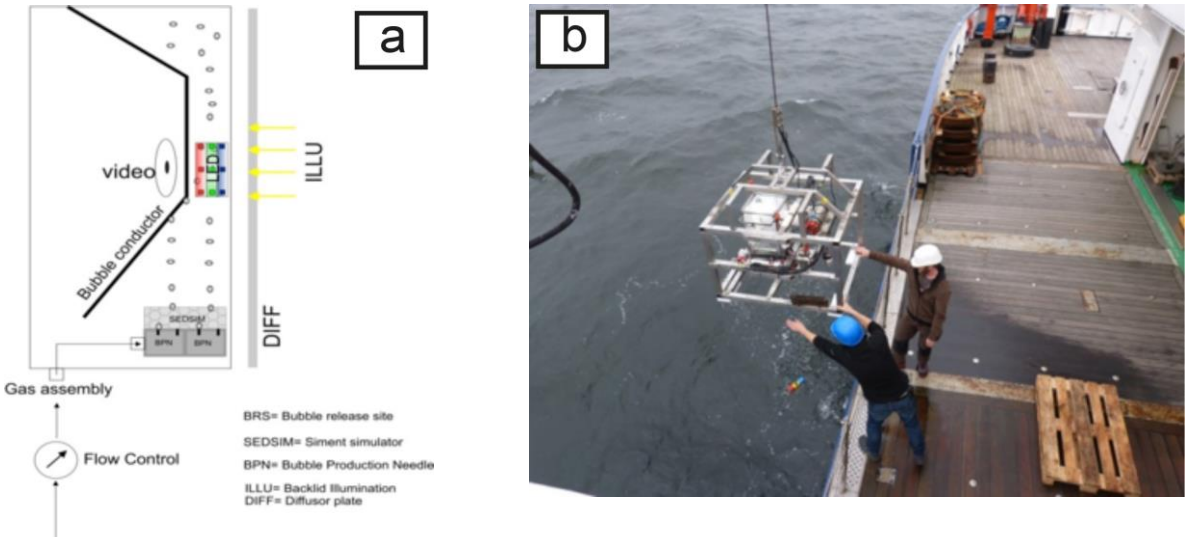

Figure 8: (a) Picture showing a sketch of the BBOX (b) Deployment of the OFOS system with the BBOX mounted therein

For quantitative bubble size determination two Go Pro Hero+ Black Edition cameras with extra power packs were attached in pressure-resistant POM housings to the BBOX for later stereographic video analyses. The lenses of these cameras were adjusted prior to the cruise to obtain a narrower field of view fixed at 80° x 60°. The video mode was set to VGA resolution to allow for fast 240 frames per second, which is vital to suppress bubble-mediated motion blur.

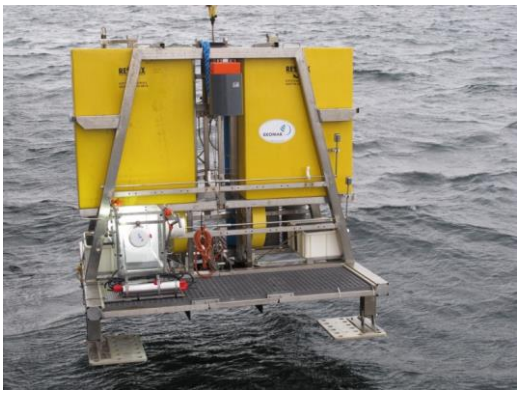

Figure 9: Deployment of the “Elevator” Lander. In the lower left of the picture the Bubble Box is visible for visualization of artificial gas bubble generation.

Preliminary Results

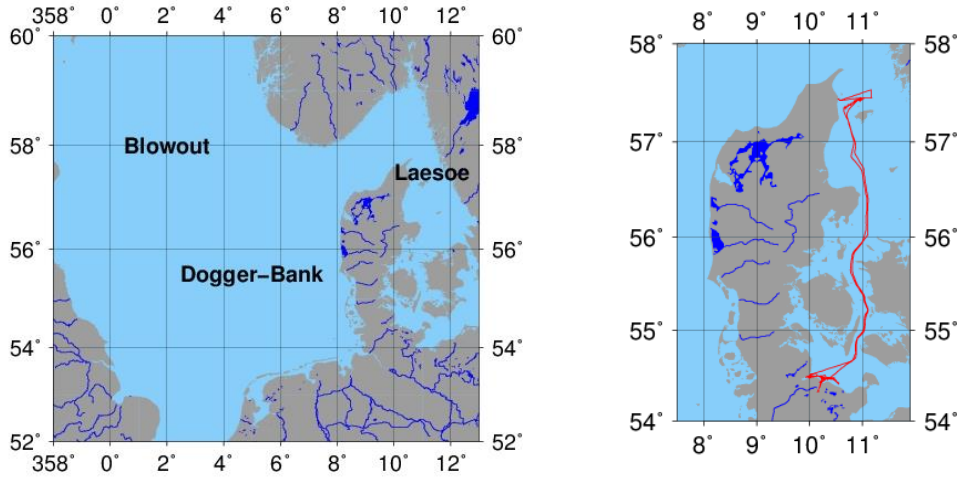

Figure 10: The originally planned research areas (left: Blowout, Dogger Bank) and actual cruise track (right, red line) of cruise AL447.

Sonar System Performance

In the beginning of the cruise the inertial motion unit (IMU) data supplied by the F180 suffered in performance due to an incomplete calibration state of the F180 heading. Moreover, the DGPS Fugro Seastar datagrams indicated frequent failure that were likely caused by the low antenna position on the mid-deck of R/V ALKOR (short cable) with potential multipath and shadow effects. Therefore the DGPS correction system was switched off after day 2 with significant improvement on the inertial navigation stability and GPS consistency. We detected severe malfunction of one of the F180 antenna cables causing a low number of identified satellites (< 5) on the secondary antenna of the F180. After repair of the damaged F180 cable plug good coverage with 9-11 satellites was realized during most of the time with GPS accuracies of ±0.5 m.

After elimination of these errors an “eight” was sailed for two hours and the heading accuracy improved to 0.15° not yet meeting specification. Therefore we decided to conduct a land-based re-measurement of the initial static offsets on day 8 and discovered a significant error of >1 m in the across track offset between MRU and primary antenna. After correcting for this initial error the system achieved full calibration within 3 hours of surveying and operated within specification for the rest of the cruise.

The multibeam system itself operated without any problems and delivered high resolution data of both research areas. A full roll-pitch-yaw (+1.68°, -5.0°, +3.9°) calibration was successfully performed with the parameters set into the online recording software SIS after day 6 and lines fit together smoothly. A re-calibration of yaw might be meaningful given the initial problems with heading initialization (several yaw lines were sailed). In the pockmark area of Eckernförde the multibeam data suffered from acoustic interference and we speculate that a concurrent acoustic monitoring device was deployed on the seabed here. A test with the CUBE algorithm was performed showing valuable results for automatic filtering these strong interferences.

The results of single beam calibrations showed the best results for 38 kHz (deviation from beam model: RMS = 0.07 dB), 70 kHz (RMS = 0.08 dB), and 120 kHz (RMS = 0.08 dB). Acceptable calibration results were obtained for 200 kHz (0.16 dB). An example of good distribution of a standard sphere within the beam is illustrated on Figure 11 below.

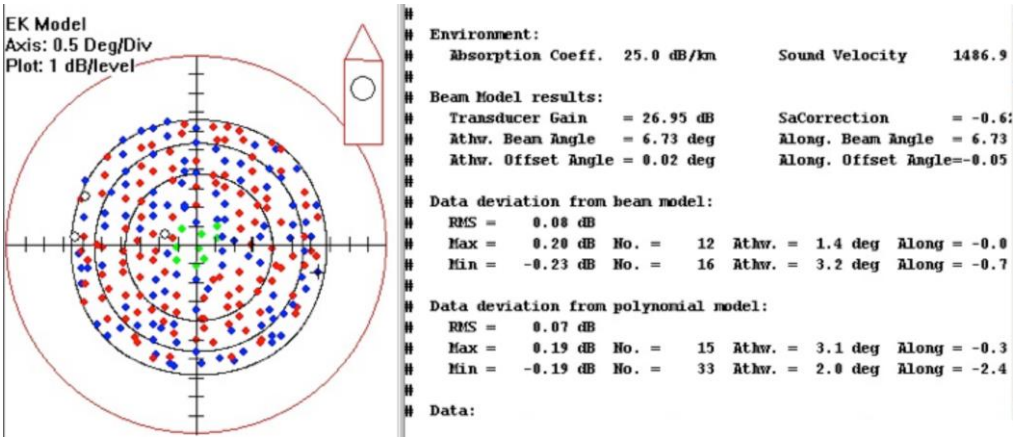

Figure 11: An example of a good EK60 calibration model. All points are located within 3 dB range. Green dots show target locations near the main acoustic center the of echo sounder. Red and blue dots show data, whose target strengths are larger or smaller in comparison to the model results. Very good calibration outcomes result in (i) symmetric distribution of targets within beam and (ii) random distributions of red and blue dots, and as a result a small deviation from the beam model (RMS <0.1 dB).

Apart from the well-known Baltic-seiche 27 hours period water level oscillation (Figure 12), vertical oscillations lasting several minutes were occasionally identified across all beams in one swath of the multibeam data during windy weather. Centre beam depth analyses were performed indicating distinct oscillations in the fft spectrum (Figure 12). Analyses of adjacent survey lines reveals that these oscillations do not represent real seabed features. Physically, the motion sensor would be capable to integrate acceleration values over 16 seconds (except with I-Heave), not longer. Therefore we speculate about local water level oscillations (seiche effects) with amplitudes of up to 0.2 m and periods lasting several minutes. Such seiches typically occur in lakes, bays, or harbors as a response of e.g. stronger wind or seismic events with oscillations in the minutes to hour scale depending on basin length and depth. As no RTK GPS solutions have been acquired, a correction for such phenomena is challenging.

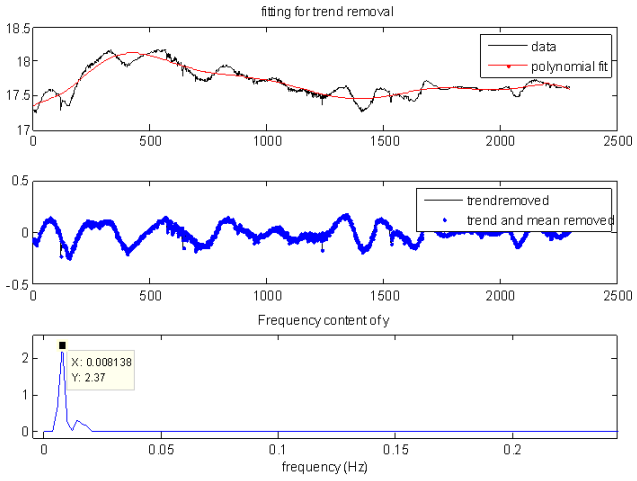

Figure 12: Water-level oscillations for the Eckernförde Bay. Upper: oscillations with polynomial fit for trend correction. Middle: trend-removed curve showing the remaining oscillations with a period of several minutes. Lower: FFT spectrum for the residual oscillations.

Bathymetric und Subbottom Gas Seepage Characterization

Pockmarks at Eckernförde Bay

The Eckernförde Bay pockmarks have been investigated in detail since decades (Whiticar, 1981; Schlüter et al., 2004), bathymetric mapping was extended during AL447 to the north and west of Mittelgrund, respectively. Pockmarks termed PM1 to PM3 hereafter (Figure 13a) were re-surveyed to investigate their morphological evolution over the past years and to detect potential gas release via flare imaging. No significant seabed features were identified apart from the pockmarks.

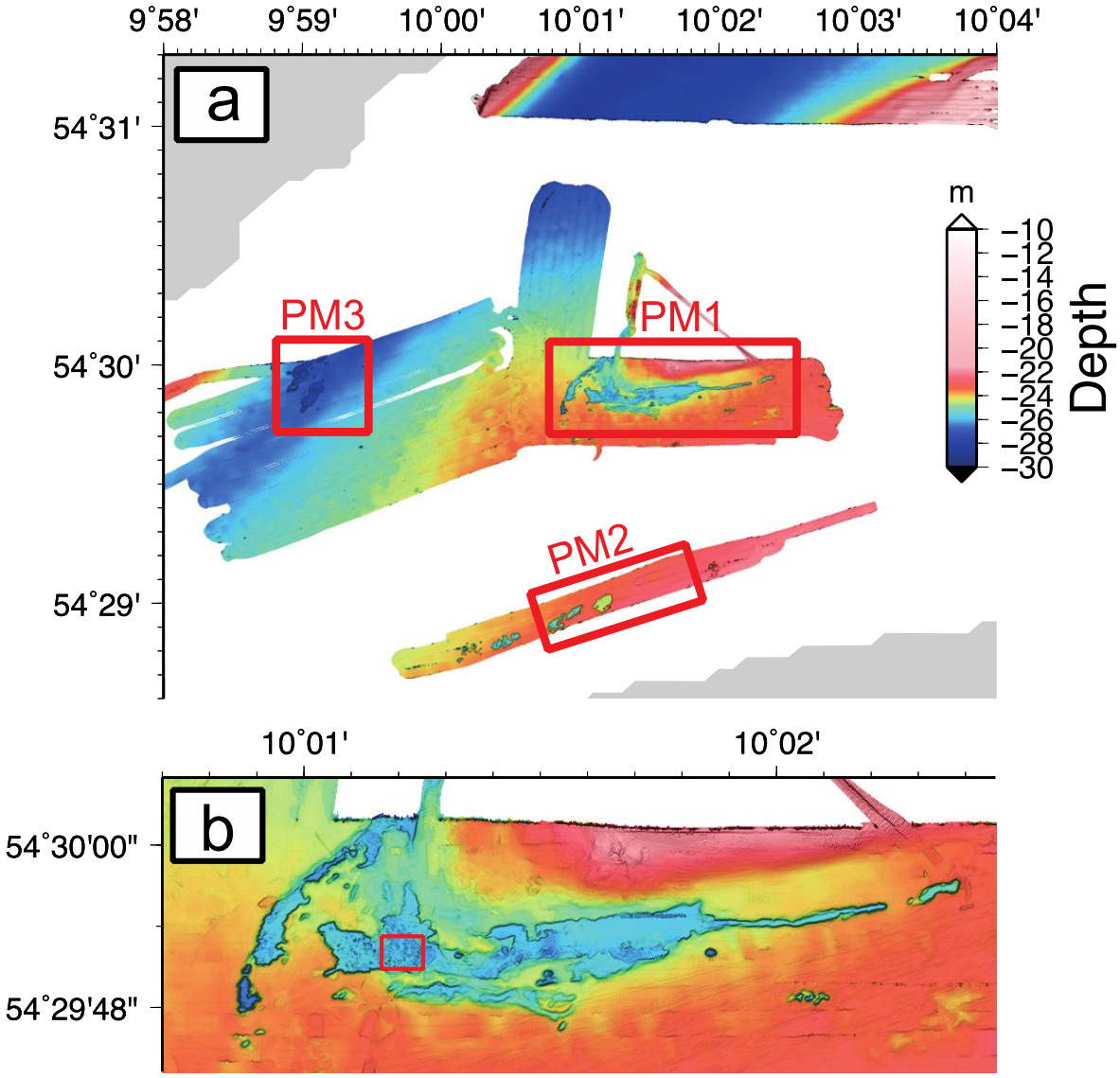

Figure 13: (a) Auto-processed bathymetric coverage chart showing pockmark areas (PM1-PM3) surveyed during AL447 in the Eckernförde Bay next to the morainic remnant "Mittelgrund". (b) Close-up of PM1, rectangle indicates the hypothetical center of highest gas release activity. Data corrected for water-level fluctuations (Figure 12) PNP (Pegelnullpunkt) 5.004 m.

Close-up comparison of data gathered during this cruise with previous measurements of PM2 is provided in Figure 14 indicating no significant morphological change. We conclude a steady state setting between sedimentation infill and gas expulsion/erosion processes balancing each other. However, thorough evaluation remains as a future task to quantitatively compare the water-level corrected bathymetric grids in regard to volume and shape differences.

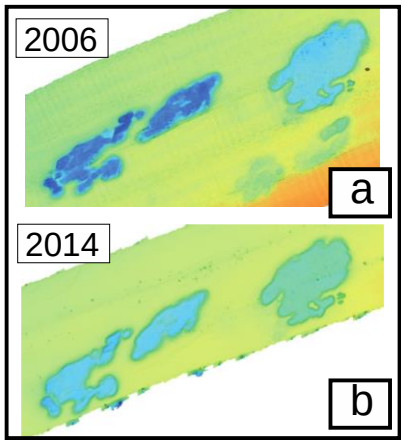

Figure 14: (a) PM2 Pockmarks recorded with ELAC 180kHz Seabeam 1180 (gathered during AL290 by J. Schneider, and (b) KONGSBERG EM2040c operated during this cruise.

Subbottom survey lines were run across PM1 and PM2 (Figure 13). The PM1 site was dominated by acoustic turbidity. Methane gas bubbles in the sediment (Wever et al. 2006) scatter and attenuate most of the incidence sound energy, preventing any further sound penetration, leading to acoustic blanking of the beneath subbottom. Therefore, it was not possible to gather information about the subbottom topography of PM1 at Mittelgrund. This so called shallow gas front mostly varies between 1.8 and 0.85 m and reaches the seafloor at several positions within the pockmark, which is in good agreement with other observations in literature (e.g. Wever et al. 1998).

In contrast, the shallow gas front was not continuous at PM2. Maximum penetration depths of up to 13 m were achieved with the 4 kHz frequency at gas free locations. These locations revealed sediment layers above glacial till (Wever et al. 1998). The glacial till topography is mostly flat with some elevations. The plains are about 3.5 m bsf. The areas between these elevations are filled with horizontal sediment layers of different depth. Again, the depth of the shallow gas front was variable and reached from depth of up to 0.9 m up to the seafloor. It mainly reaches the seafloor within the pockmarks of PM2. The distributions of the shallow gas horizon around PM1 and PM2 are shown in Figure 15.

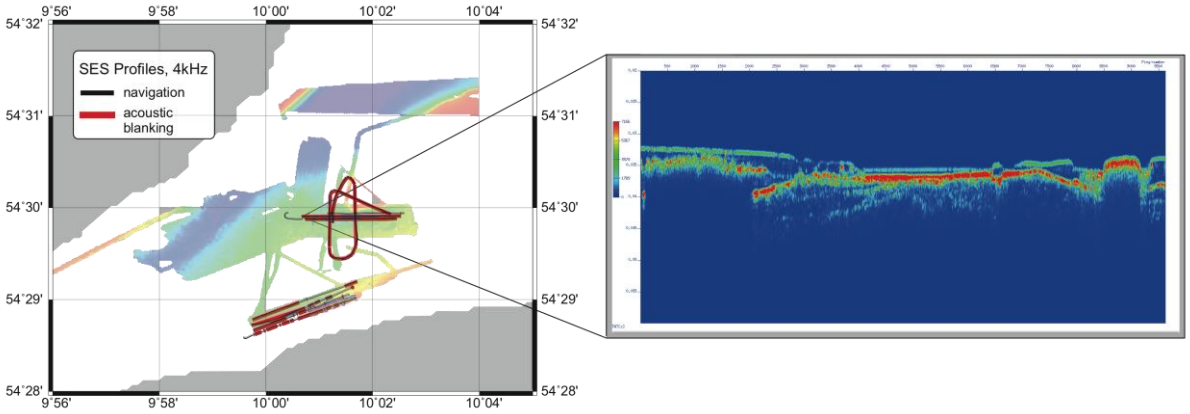

Figure 15: SES profiles run across PM1 and PM2 (Figure 13) plotted onto the bathymetry. Inlet shows the SES 4 kHz echogram running from west to east crossing PM1.

Carbonate Reefs off Læsø

The area north of Læsø belongs to a protected *NATURA 2000* area and is characterized by different habitats such as boulder reefs, sandbanks, and 'bubbling reefs' formed by leaking gas and mineral precipitation. The gas seep sites are characterized by bathymetric highs built of carbonate (Jensen et al., 1992). Six sites with approximately 0.8 m elevation and 50 m width were identified in our surveyed area (Figure 16), where some of them were not known to exist before (pers. Comm. J.B. Jensen). At one reef in the northwesterly survey area acoustic evidence for distinct gas bubbling in the form of individual bubble streams (Figure 16) was found. To complete previous work performed by our Danish colleagues, subbottom survey lines were run across the observed gas seepage and perpendicular to the reef slope (Figure 17). At this site, the geological strata appears rather complex, requiring further evaluation. The data will be shared with our Danish colleagues to complete their *NATURA 2000* habitat mapping goals.

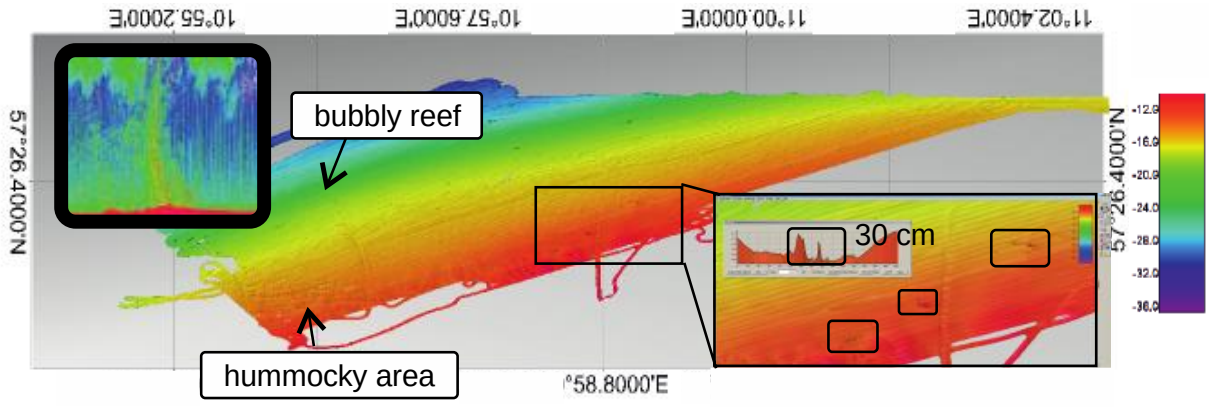

Figure 16: Survey area north of the island Læsø (Kattegat). Inlet highlights the carbonate mounds (reefs) and respective gas ebullition above

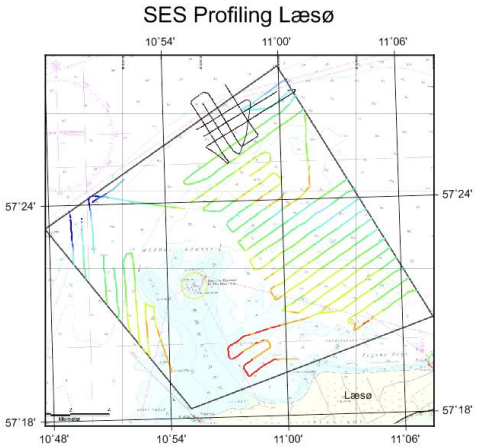

Figure 17: Overview of AL447 INNOMAR subbottom tracks run off Læsø during AL447 (black lines) to complete previous surveying from our Danish colleagues (coloured lines provided by courtesy of Jörn Bo Jensen).

Flare Imaging and Gas Bubble Monitoring

Acoustic gas seepage detection and characterization via acoustic 'flare imaging' was one major goal of the cruise. Dedicated surveys were performed to investigate the water column, therefore, all concurrent echosounders (navigation sounders, ADCP) of R/V ALKOR were switched off to avoid possible acoustic interferences and survey speed was reduced to 1-3 knots. The multibeam flare imaging technology was applied for high tempo-spatial resolution and broad coverage of gas seepage in the water column (Schneider von Deimling and Weinrebe, 2014), whereas the single beam EK60 was used to obtain absolute sonar target strength that is needed for bubble size determinations and flux estimates. For the EK60, each transect was divided into several segments of similar distances strength (40–70 m) via visual inspection of the echograms for changing bubble/non-bubble densities. The segment distance must also be large enough to provide a sufficient number of detections for accurate approximation of total strength distributions of the various targets.

The bubble/non-bubble separation (BNS) method first calculates an approximate target strength distribution of all targets in the sample volume (F_{a*}) by relating the target strength distributions for all identifiable bubbles (F_b) and identifiable non-bubbles (F_{nb}) with a factor that describes the approximate proportion of bubbles (A_b) and non-bubbles ($1-A_b$) in the sample volume:

$$F_{a*} = F_b \times A_b + F_{nb} \times (1-A_b). \qquad (1)$$

First, bubbles and non-bubbles can be distinguished based on rise velocity. Bubbles appear as diagonal tracks in echograms with a rise velocity between 15 and 50 cm s^{-1}, while non-bubble tracks remain horizontal with almost no vertical velocity component (or <15 cm s^{-1}). F_b and F_{nb} were then found by computing the bubble and non-bubble frequency distributions. F_{a*} and F_{nb} are only approximations of the target strength distribution of various types of targets because they are based on the number of identifiable targets (bubbles and non-bubbles, respectively) for each target strength bin, which is less than the total number of detected targets (i.e., $F_{a*} > F_b+F_{nb}$). The latter is related to the fact that rise velocities cannot be accurately computed for short tracks. Ultimately, we aim to find the F_{a*} that most closely matches the true F_a, and this is dependent on finding the appropriate A_b. The most appropriate A_b is found by testing all possibilities (between 0 and 1) in Eq. 1 and choosing the one that allows for the best correlation between F_{a*} and the real F_a. For more details regarding this analysis see Ostrovsky (2009).

Natural Gas Seepage at Eckernförde Bay

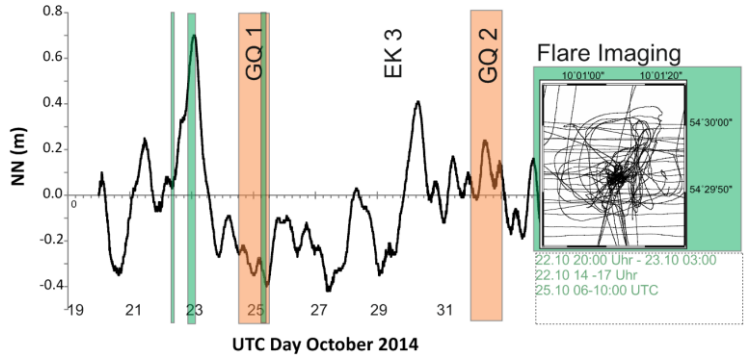

Figure 18: (Left) Water-level fluctuations for the end of October 2014 in the Eckernförde Bay used for water-level correction (pegelonline.wsv.de). Highlighted times show flare imaging with the respective device. (Right) Flare imaging survey lines during highlighted times.

Hundreds of gas bubble release events were identified with sonar measurements in the vicinity of PM1. We hypothesize that the gas discharge originates from the shallow biogenic gas hosted in the muddy sediments identified earlier (Wever et al., 1998) and during this cruise by acoustic blanking (Figure 15). The release character of gas bubbles fed by shallow gas deposits in the muddy sediments of the Eckernförde Bay are likely sensitive to pressure changes (Jackson et al., 1998; Schneider von Deimling et al., 2010). PM1 and PM2 (Figure 13) were thus repeatedly surveyed during different water levels (Figure 18). Jackson et al. (1998) provided evidence for near bottom releases of free gas bubbles in the Eckernförde Bay by acoustic monitoring. First analyses with our powerful flare imaging devices (multibeam, single beam, GasQuant II) support those indications and provide unambiguous evidence for widespread release of individual gas bubbles in the vicinity of the pockmark area (Figure 19).

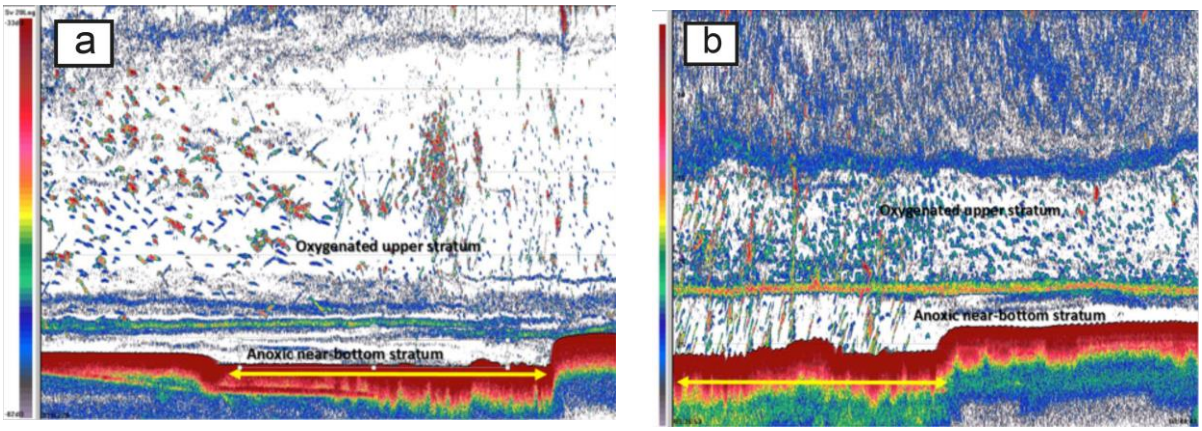

Figure 19: Echograms of the water column and bottom (red) at (a) high (Oct, 22, 2014, 22:25 UTC) and (b) low water levels (Oct, 25, 2014, 08:36 UTC). At high water level no bubble emission was detected in the pockmark (yellow arrow line). At high water level a large amount of bubbles (inclined lines) are emitted from the pockmark. Anoxic conditions below the pycnocline (a thin yellow-reddish horizontal layer) allow to see the only bubbles in the low near-bottom stratum, while fish and bubbles exist above the pycnocline.

The data shows large spatial and temporal variability in bubble emission from the bottom, which on the one hand is influenced by changes of hydrostatic pressure at the bottom (water level changes) and on the other depends on availability of large amounts of bubbles in the surface sediments in the pockmark, which is apparently associated with accumulation of large amounts of organic material and its anaerobic decomposition.

Number of bubble releases, rise height, and rise velocity of the bubbles can be assessed by evaluating the sonar bubble rise data pattern, i.e. “rising lines” (Figure 21a and Figure 25). A subset of the data gathered at different water level phases (Figure 18) was analysed and first results suggest a distinct correlation between gas seepage activity and water level phase with a maximum gas release during water level low. The gas bubble events have been preliminary investigated by searching for rising gas bubbles in the stacked view of the water-column data. Accumulations of rising gas bubbles have then been tracked in the fan view of the water-column by picking time, depth and coordinates for individual bubbles. Afterwards, rise velocities have been estimated using the change in depth (Δz) for the tracking interval (Δt). First results for 53 picks in the center of PM1 (Figure 13b) show a mean bubble rise velocity of approximately 0.23 m/s (Figure 20). Gas bubble sizes will be estimated by the relationship between bubble radius and measured rise velocity after Clift et al. (2005) and compared with acoustically determined bubble size (EK60).

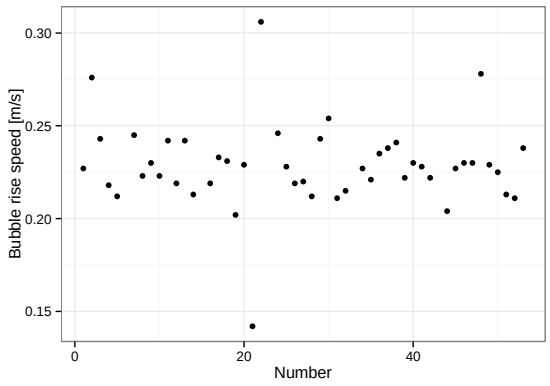

Figure 20: Bubble rise velocities for 53 different bubbles derived from tracing in the fanview of the EM2040c multibeam.

The finding of the release of much larger bubbles compared to Jackson et al. 1998 is supported by the 0.23 m/s mean rise velocity and verified by our BBOX tow track, where naturally released gas bubbles could be captured on video (Figure 21c). Later stereo video data processing of the two GoPro camera videos integrated in the BBOX will allow for a very accurate determination of the bubble size and the flux. Further analyses of the calibrated single beam data will later allow for real target strength measurements in dB and quantitative bubble size estimates.

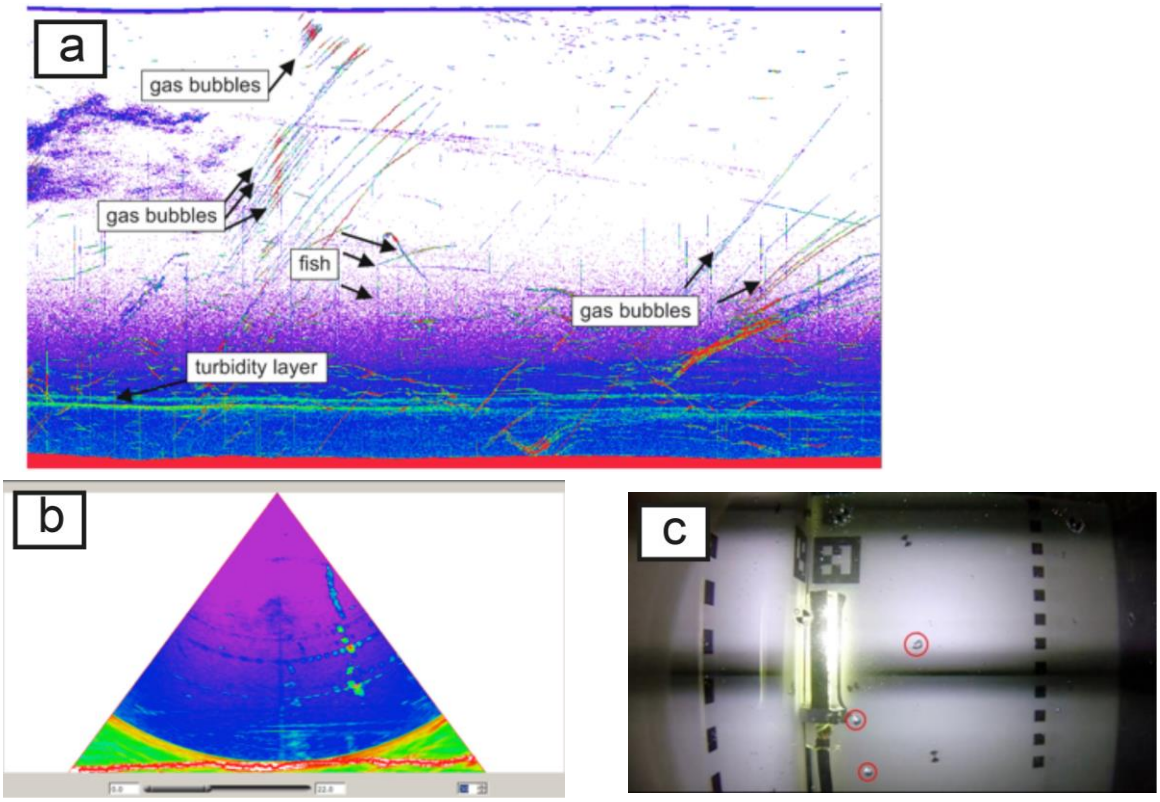

Figure 21: (a) Beamstack echogram of EM2040c data. “Rising lines” represent acoustic patterns of rising gas bubbles (b) example showing a beamfan view with gas release at the starboard side similar to the online data of the multibeam (c) in-situ optical snapshot of naturally released gas bubbles in Eckernförde Bay.

After remote detection of gas bubble seepage by shipborn sonar, the GasQuant II system was deployed for in situ measurements twice in PM1 for approx. 24 hours each. The system’s setup was slightly varied to find optimal settings for gas detection (Table 3). Additionally a GoPro camera was attached to the system to gain information about the landing of the device on the sea floor.

Table 3: Setup and remarks of the GasQuant II system deployments at Eckernförde Bay

Nr.	Time (UTC)	Position	Setup	Remarks
1	24.10.2014 13:19 to 25.10.2014 12:19	54° 29.913', 10° 1.269' Eckernförde PM1	15° forward looking pingrate 5 Hz range 100 m pulse length 600 µs	lander slowly sunk into mud; finally fallen on the seafloor
2	01.11.2014 14:25 to 02.11.2014 13:55	54° 29.878', 10° 1.226' Eckernförde PM1	90° upward looking pingrate 5 Hz range 40 m 2 ping setups serially: pulse lengths 240 µs 600 µs	two pulse lengths have been set in alternation (saved in different files)

For the first deployment in the PM1 pockmark of Eckernförde Bay (Figure 13), the lander was set up to look forward with a horizontal swath. However, one foot of the lander sank into the mud over

time and finally the transducer was orientated upside up. Subsequently, GasQuant II accidently operated in an upward looking mode. During this time many single bubbles could be detected rising from the seafloor (data not shown).

A second deployment of GasQuant II was conducted with perforated metal plates to avoid sinking into the sediment. To optimize the resolution, a range of 40 meters was used for an upward looking deployment. The dataset shows many single rising bubbles that can be separated clearly from other signals like fish that preferentially move horizontally instead of vertically (Figure 22).

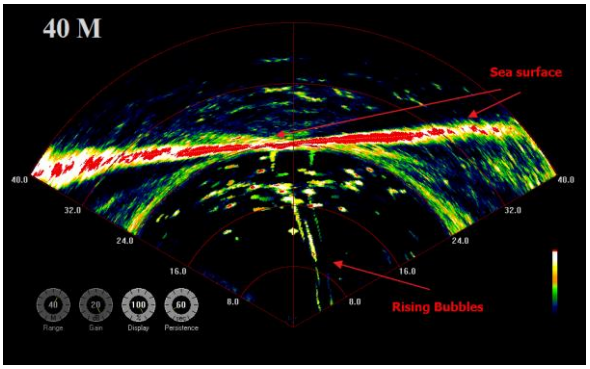

Figure 22: Imagenex in upward looking mode at Eckernförde Mittelgrund. To make the rising bubbles more visible, datapoints have been set up to stay persistent for 60 seconds. While fish move mostly horizontally, rising bubbles can be clearly distinguished by their vertical movement.

First investigations in the stacked view of FMMidwater show fluctuations of the amount of bubbles rising per time. Detailed correlation of the dataset with the water level will be available in post processing.

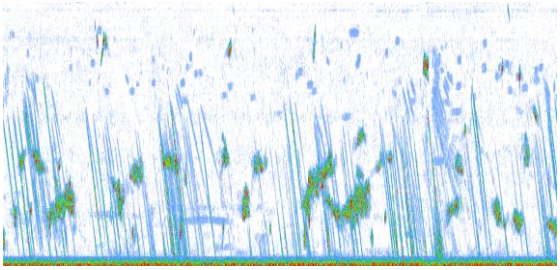

Figure 24: Fledermaus stacked view of the Imagenex data; Half an hour of data (02.11.2014 14:53–15:23); Example for a time with many bubbles rising.

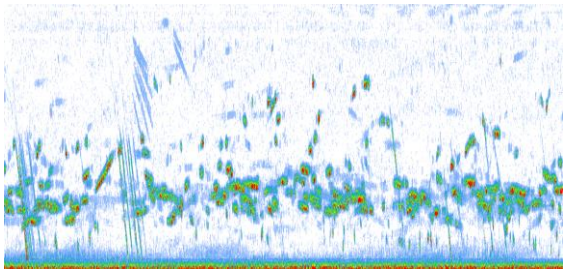

Figure 23: Fledermaus stacked view of the Imagenex data; Half an hour of data (02.11.2014 21:25–21:55); Example for a time with small amount of bubble rising.

Bubbling Reefs off Læsø

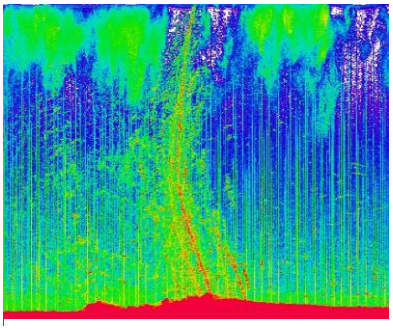

Figure 25: Stacked beam presentation of EM2040c multibeam data showing gas release of several individual bubble chains rising through the water.

Flare imaging off Læsø only revealed one active gas releasing spot (Figure 25), however, complete sonar data review has not yet been performed. The active gas release spot appears on top of a 0.5 m bathymetric high. Most likely this represents one of the previously documented bubble reef carbonate structures as has been reported for the Kattegat elsewhere (Jensen et al., 1992). More mound structures were identified in the surveyed area (Figure 16) and analyses of the respective multibeam WCI data might expose further sites with active gas release.

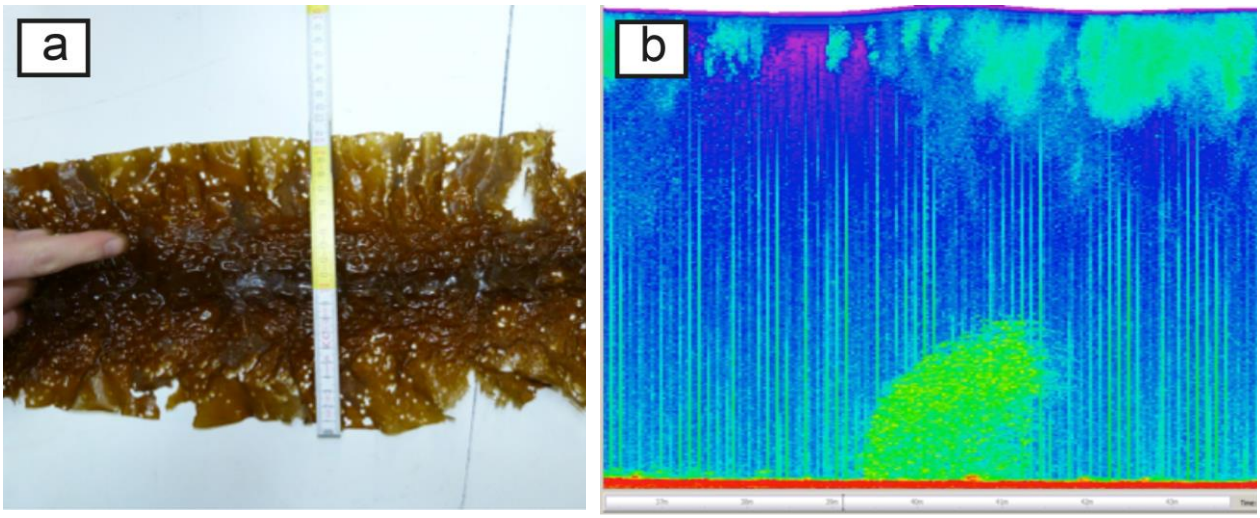

Figure 26: (a) Picture of an algae leaf that was wrapped around the GasQuant II device after recovery from the deployment off Læsø position (b) sonar picture potentially showing an algae "forest" on the seafloor.

GasQuant II was deployed at the bubble site (Figure 25). Due to the sandy seafloor the lander stood stable, but the data show strong and constant signal returns superimposed with noise. After recovery a large algae leaf was wrapped around the GasQuant II device (Figure 26a). We hypothesize that the GasQuant II was deployed in an area highly populated with large algae. As a result near range backscattering from the algae might have caused severe sonar signal attenuation. As a consequence no bubbles were detected in the GasQuant II records at all. The idea of algae signal attenuation is also supported by the shipborn sonar data showing stationary features with elevated sonar strength emanating from the seafloor up to 3 m high (Figure 26b).

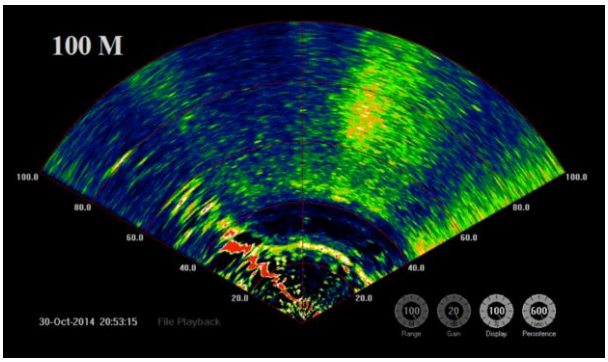

Figure 27: Imagenex data from the deployment at Læsø. The image does not change notably during the 23 hours of data. To visualize the noise effects better, data points have been set up to persist for 600 seconds. Apart from noise no useful data could be extracted from the dataset.

Table 4: Setup and remarks of the GasQuant II system deployments at Læsø.

Nr.	Time (UTC)	Position	Setup	Remarks
1	30.10.2014 14:17 to 31.10.2014 13:17	57° 26.263', 10° 56.544' Læsø	5° forward looking pingrate 5 Hz range 100 m pulse length 600 µs	Lander potentially looked into algae forest, data not useful

Artificial Gas Release

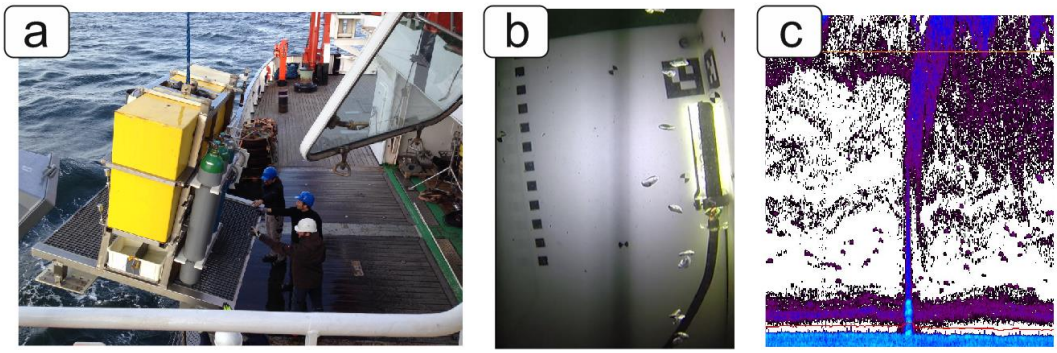

Figure 28: (a) Deployment of the gas emitting module and the BBOX with the use of the Elevator lander on cruise AL447 (b) in-situ shots of artificially produced gas bubble emissions (c) acoustic image of the water column (14 m) and the artificially induced gas flare using the EK60 on 38 kHz.

An artificial gas release system was deployed at 14 m water depth close to the Kiel Fjord to generate a calibrated gas bubble flux on the seafloor (Figure 28a). Argon bubbles were released through a nozzle with 4 mm radius to produce single gas bubbles (Figure 28b). Subsequently EK60 survey lines were run across this in situ gas release flux to obtain the sonar backscatter. This data will then be used to validate model predictions about the relation between gas flux intensity and sonar backscattering strength. However, it was very challenging to navigate the narrow beam precisely above the release site at this shallow water depth, therefore, only a few records cover the gas release (Figure 28c).

The Lander experiment was designed to produce bubble plumes of known intensity and to measure the backscattering intensity with the EK60 echo sounder for flux calibration purposes (Figure 29). The position of the lander at shallow depth (~14 m depth, due to safety reasons) determined large difficulties of its detection with the vertically oriented narrow beam, since the beam width at the maximal detection depth (<12 m) is very narrow.

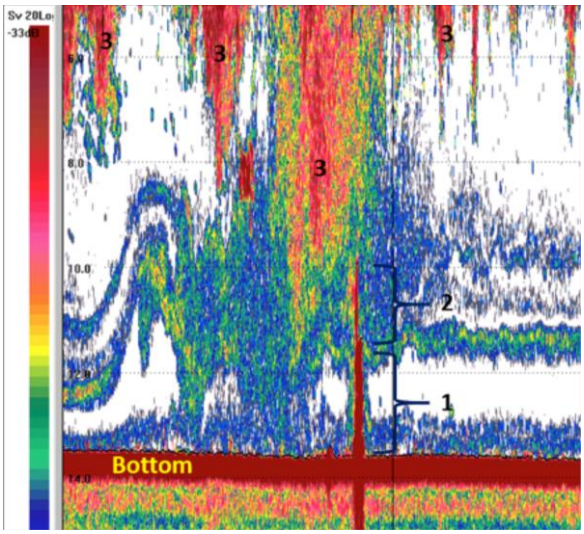

Figure 29: Lander experiment to create and detect artificial bubble plumes of known bubble emission intensity. (1) Lander body (~2 m height), (2) bubble plume emitted above the lander, (3) surface bubbles entrained due to wind and ship movement.

Chemical and Microbial Seepage Characterization

Methodology

Dissolved CH_4 Analyses

For analysis of methane concentrations and MOx rates at discrete water depths, we sampled the water column with a 12 × 10-liter PTFE-lined CTD/Rosette sampler and sub-samples were taken immediately upon recovery of the sampler. For methane concentration measurements, water was subsampled into 120 ml glass vials through silicon tubing allowing ~300 ml to overflow before crimp-top sealing the vial bubble-free with thick butyl rubber stoppers. Subsequently, a high-purity nitrogen headspace (5 ml) was added and the samples were fixed by adding 5 ml of aqueous NaOH solution (30%, w/v). Samples were shaken vigorously and allowed to equilibrate for 24 hours before subsampling 200 µl headspace with a gas tight syringe for analysis. Similarly, atmospheric methane concentrations were analysed from 500 µl of air sampled at ~2 m above the sea surface at the luv side of the ship with a gas tight syringe. Methane concentrations were determined on board by gas chromatography (Hewlett Packard 5890 Gas Chromatograph equipped with a 80/100 mesh HayeSep Q packed stainless steel column (1.83 m length, 2 mm i.d.) and a flame ionization detector. The system was operated isothermally at 60 °C with N_2 as carrier gas at a flow rate of 30 ml/min). Calibration was performed with a 100 ppm methane standard (Air Liquide, Germany), and reproducibility determined by analysis of triplicate subsamples was less than ±5%. Seawater methane concentrations and the degree of saturation with respect to the atmospheric equilibrium were calculated with consideration of sample and headspace volume, temperature, salinity, atmospheric pressure and atmospheric CH_4 mixing ratio (Wiesenburg and Guinasso, 1979).

We also collected samples for analysing the stable carbon and hydrogen isotope composition of dissolved methane in our shore based laboratories. For this approach, sea water was sampled analogously as for methane concentrations in 2.5 l glass bottles, sealing the bottle bubble free with thick butyl rubber stoppers, subsequently adding a 20 ml N_2 headspace and fixing the samples with 20 ml NaOH solution.

Microbial Activity and Identity

Aerobic methane oxidation (MOx) proceeds according to:

$$CH_4 + 2\ O_2 \rightarrow CO_2 + 2\ H_2O$$

MOx rates were determined at sea from ex situ incubations with trace amounts of tritium labeled methane (C^3H_4), allowing to trace the label transfer by measuring the activity of substrate (C^3H_4) and product pools (^3H_2O) after incubation (Berndt et al., 2014; Niemann et al., in press). For each sampling depth, three 20 ml crimp-top vials were filled and closed bubble-free with bromobutyl stoppers (Helvoet Pharme, Belgium). Subsequently, each sample was amended with 10 µl gaseous C^3H_4/N_2 mixture (~25 kBq, <50 pmol CH_4, American Radiolabeled Chemicals, USA) and incubated for 72 hours at in situ temperature in the dark. The incubations were terminated by unsealing the vials and immediately subsampling 2 ml of the incubation medium and determining the radioactivity of both, the remaining C^3H_4 and the produced ^3H_2O by liquid scintillation (Hidex Triathler LSC counter, Hidex, Finnland). A 10 ml aliquot of the remaining incubation medium was then amended with aqueous NaCl solution (20%, w/v) and purged for 30 minutes with air to strip out the remaining methane. The activity of the produced ^3H_2O was then determined from a 2 ml aliquot by liquid scintillation. MOx rates were corrected for (insubstantial) tracer turnover in killed controls (fixed with

100 µl, saturated HgCl solution). MOx rates were calculated from the fractional turnover of labelled CH_4 and water column CH_4 concentration assuming first order kinetics (Reeburgh, 2007):

rMOx = k×[CH4]

where *k* is the first-order rate constant (determined from the fractional turnover of labeled CH_4 per unit time and corrected for tracer turnover in killed controls) and [CH4] is the concentration of CH_4 at the beginning of the incubation.

Additional samples were collected for determining the identity and abundance of key microbial communities through fluorescence in situ hybridisation (FISH) (Pernthaler and Pernthaler, 2007). For this, 100 ml of aqueous sample were fixed with 5 ml formaldehyde solution (30%) for 1-4 hours at 4°C. Subsequently, samples were filtered through polycarbonate filters (0.2 µm pore size) rinsed with deionised water and stored at -20°C until further analysis in our home laboratories.

CH_4 Air Sampling and Meteorology

Atmospheric concentrations of the greenhouse gases CO_2 and CH_4 were continuously monitored on R/V ALKOR. Three air intakes for these measurements where installed at the ships bow, above the bridge and in the mast, and then routed into the wet-lab. Thereby measurement of concentration gradients allow for later sea-air gas flux assessments. Respective side parameters needed for such flux calculations, i.e. wind speed and water temperature were logged via the WERUM DVS data system throughout the cruise. The gas measurement system consists of a cavity ring down spectrometer Picarro G2301-m and GEOMAR's 'Atmospheric Intake System' (AIS) that pumps air from the air intakes into integrator volumes, and then towards the Picarro spectrometer. Samples from each intake level are measured one after the other. Analyzing time was set to 1.5 minutes per level. The gas concentration measurements could be examined in real time with the Picarro software (Figure 30) and subsequently sent to a laptop computer running OFOP (Ocean Floor Observation Protocol). OFOP is able of logging the measurement data, adding the corresponding ship position and the current air-intake number to separate the air intake signals in later post-processing analysis. Additionally OFOP can plot the data on top of any georeferenced map in real time.

Figure 30: Atmosphere intake system (AIS) with the Picarro measurement control computer (right computer screen) and the OFOP data logging computer (left notebook) in the wet-lab.

Table 5: Air intake elevation and delay

Air intake nr.	Position	Elevation above sea level [m]	Tube delay [min]
1	Peildeck	10.51	01:37
2	Mast	16.29	01:34
3	Bug	5.47	02:30

Due to the long tubing between AIS and the air-intakes, there is a time offset between the gas measurement and air sampling. This delay was measured with the help of a timer and a person creating a discrete breath-signal pulse at the different air-intakes; depending on tube length and pump speed, a CO_2 peak could be identified after 1.5 to 2.5 minutes. The elevations of the three different air intakes have been measured with laser distance measurements from shore. The results of these measurements are summarized in Table 5.

Preliminary Results

Water Column Methane Concentrations and Activity of Aerobic Methanotrophs

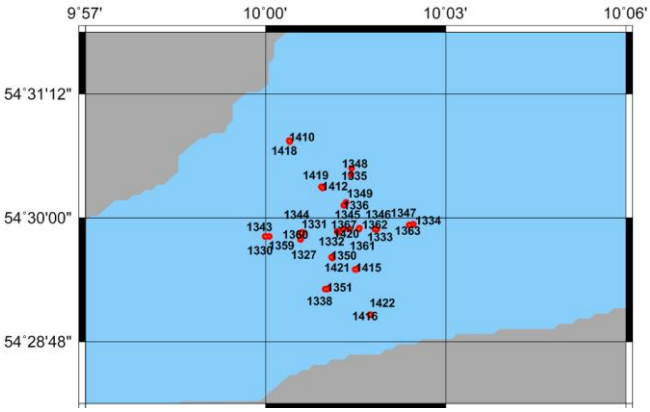

Figure 31: Overview of CTD Stations in the Eckernförde Bay

Eckernförde Bay

We observed highly spatiotemporal variations in water column methane contents and MOx activity on very short time scales of hours to days. Anoxic bottom waters in a trough in the northern part of the bay contained extremely high methane concentrations of up to 800 nM, almost four times higher than long-term time series measurements reveal for the nearby Boknis Eck area (Bange et al., 2010), and on the same order of magnitude as measurements in the deep basins of the Baltic Sea (Schmale et al. 2010). The concentration sharply declined at the midwater redox interface (methane remained supersaturated with respect to the atmospheric equilibrium throughout the water column at all times) (Figure 32 and Figure 33). The methane decrease at the redox interface was related to highly active MOx communities consuming methane under microoxic conditions at rates of up 40 nM/d. About 12 hours later, the methane content and the extent of bottom water anoxia was much lower and MOx activity was highly reduced in the northern part, but strongly elevated in the southern part of the bay.

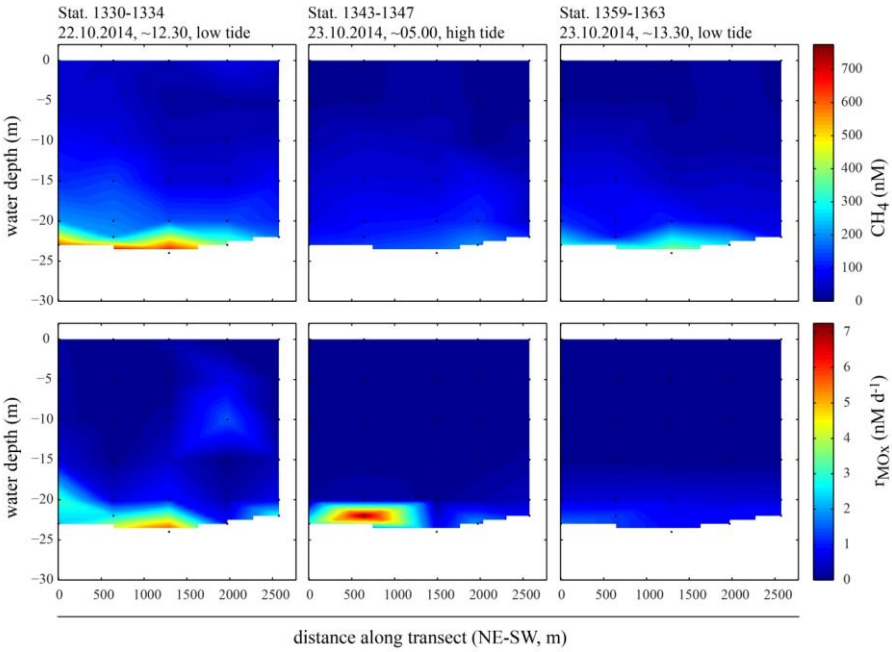

Figure 32: Methane concentrations and MOx rates along a NE-SW transect crossing Eckernförde Bay. Methane concentrations were generally highest in hypoxic/anoxic bottom waters where MOx proceeded under microoxic conditions. Note the high spatiotemporal variability of methane and MOx.

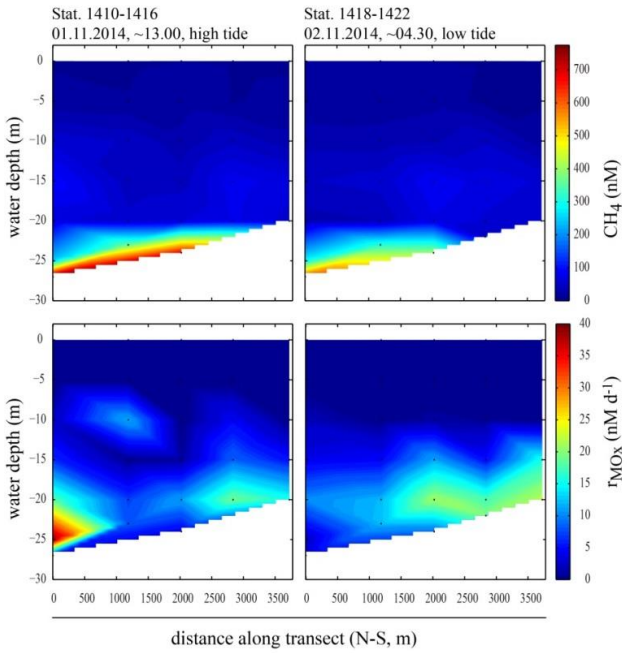

Figure 33: Methane concentrations and MOx rates along a N-S transect crossing Eckernförde Bay. Methane concentrations were generally highest in hypoxic/anoxic bottom waters where MOx proceeded under micro-oxic conditions. Note the high spatiotemporal variability of methane and MOx and the apparent independence of methane concentrations and MOx rates (note that MOx was about 5-fold higher compared to the late October sampling; Figure 32)

Læsø

Methane concentrations at the bubbling reefs of Læsø were very low, typically at background levels (~4 nM) and only a few samples showed slightly elevated methane contents (up to 13 nM; data not shown). Because of the low methane contents (probably as result of strong currents and rapid dispersal), no MOx rates were measured.

Atmospheric Measurements

With the exception of small interruptions for system maintenance reasons, the atmospheric concentration measurements were performed throughout the entire cruise. First analyses show increased gradients above active methane seepage sources at Eckernförde Bay in accordance to the flare imaging results.

However, the gradient resolution strongly decreased with increasing wind speed due to atmospheric mixing with relatively low methane concentrations in air. Especially the Picarro-transect off Læsø does not show any noticeable gradients, but rather wind induced land sources. It will therefore only be revealed in post-processing which data can be used for meaningful analysis.

Oceanography

Methodology

CTD

Salinity, temperature, depth profiles were recorded with a CTD rosette water sampler system. The CTD also provides online calculated sound velocity values. The rosette consists of 12 water bottles à 10 l which can be manually closed at the desired depth. The system was normally lowered and heaved with a speed of 0.2 m s^{-1}. At the "Kolberger Heide", a munition dumping side, it was only lowered down to about 2-3 m above the seafloor for safety reasons.

Sound velocity profiles were required for the multibeam and SES measurements. Water samples of different depths were taken in addition to the CTD-profiles at detected seepages. On board, the water samples were subsequently further analyzed for the chemical and biological components. Overall, 58 CTD casts were taken during the cruise.

ADCP

Water current measurements were conducted using a 300 kHz Teledyne RDI Workhorse Sentinel Acoustic Doppler Current Profiler (ADCP) mounted in the moonpool of R/V ALKOR. The ADCP was mounted with an offset of 45° towards the common configuration of ADCPs (Figure 34).

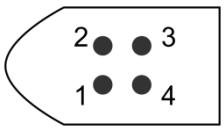

Figure 34: ADCP Beam orientation

ADCP measurements are often noisy requiring data averaging over longer time. Therefore data from several pings are integrated into an "ensemble" to assess the current velocities in x, y, and z (depth) direction. A bottom track mode was applied to measure the ships self-speed over the ground and to later separate this motion from the particle drift itself.

The ADCP recording system was supplied with navigation and compass data from a GPS system. Compass data revealed a huge offset of 272° compared to the ships compass. The ADCP was mounted next to the EM2040c multibeam in a depth of approx. 5 m water depth. According to the system the first cell range that is possible to measure was 2.95 m. The depth of the first water layer to be measured was therefore approx. 8 m.

Preliminary Results

Saline dense water with low methane concentrations enters the Kattegat at depth from the North Sea flowing through the Belt Sea towards the Western Baltic Sea and further east. A saline rich bottom layer was identified in the Kattegat at St. 1378 (Figure 36a) with 5 m thickness. Tidal and wind mixing can change the oceanographic setting in this area on short tempo-spatial scales as visible in the succeeding hydrocast (Figure 36b). Further south towards the Belt and the German

coast the tidal effects decrease. However, the hydrographic setting remains complex with extensive tempo-spatial variations. E.g. Figure 35 shows hydrocasts gathered at Eckernförde Bay only ~1 nautic mile away from each other with significant variability. Those variations have strong effects on the sound speed in the water and distribution of methane concentrations thus highly affecting later measurements.

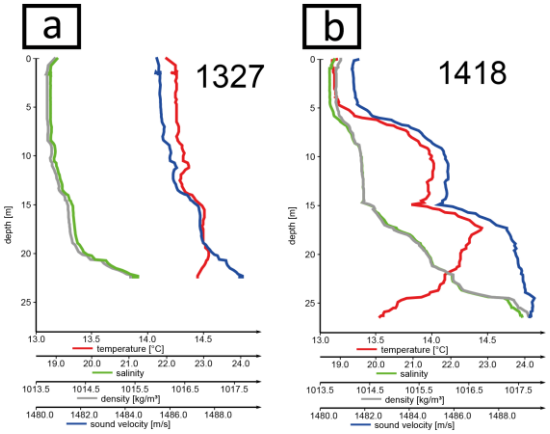

Figure 35: Two CTD casts in Eckernförde Bay showing maximum variability. Time and distance between the two are 11 days and 4 hours.

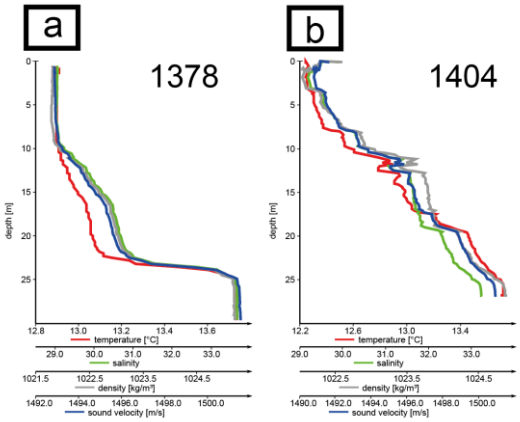

Figure 36: Two CTD casts off Læsø showing maximum variability. Time between the two are 3 days and 21 hours.

Eckernförde Bay

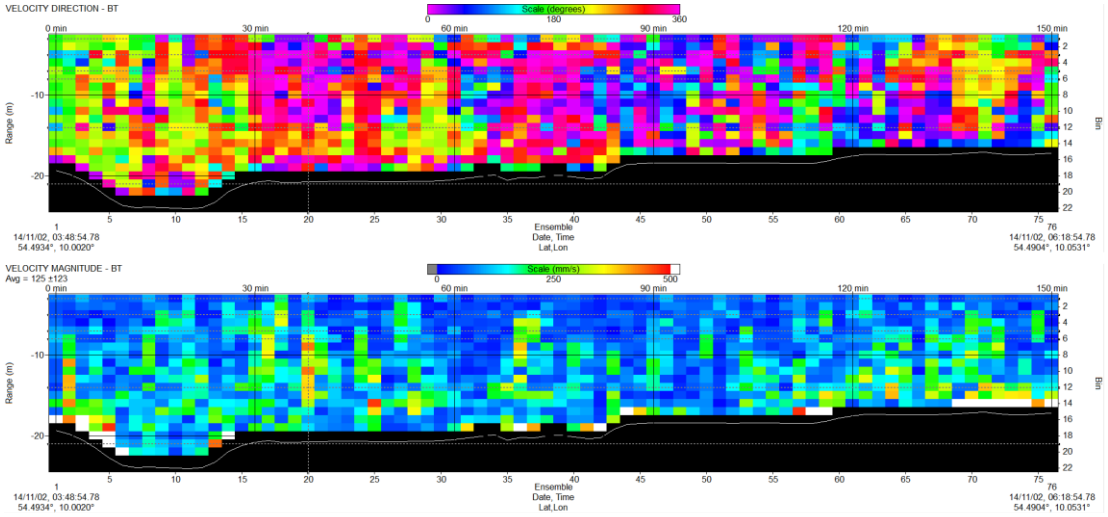

Figure 37: Short term averaged (2 min.) data from CTD transect at Eckerförde Mittelgrund. Upper: velocity direction (0 = North). Lower: velocity magnitude. Velocities are referenced to the bottom track measurements.

The ADCP strongly interfered with the EM2040c multibeam system. It was therefore not possible to run both systems at the same time. The ADCP was turned on for short time periods between multibeam survey lines and during the CTD stations and transects. Figure 37 shows the short term averaged (STA) time series of the last CTD-transact on November 2nd, but no predominant speed or direction components can be discriminated against the noise. Better results from longer averaged data are expected after post processing.

Although a first ADCP data review is missing predominant currents, we hypothesize that currents were significantly affecting the data sampling. The generally windy period caused significant water level fluctuations (Figure 18) that likely caused distinct currents during certain times.

Mapping Dumped Munition at the "Kolberger Heide"

Prior to the cruise a cooperation agreement was made between GEOMAR and the "Ministerium für Energiewende, Landwirtschaft, Umwelt und ländliche Räume" (MELUR). By courtesy of Claus Boettcher (MELUR) approximate positions of and research permissions for dumped munition sites off the "Kolberger Heide" were provided. Thus, a baseline study about the feasibility of using a novel ship-based multibeam sonar for dumped munition detection could be conducted. First analyses of the survey data support the idea that dumped munition can be clearly detected with the sidescan capabilities of modern ship-based swath sonar (Figure 38). The advantage of multibeam over conventional towed side-scan is a much better positioning of multibeam soundings with a centimeter to decimeter accuracy at high survey speeds. For safety issues, exact positions of suspicious features visible in Figure 38 are not provided in this report. Bathymetric data were acquired in parallel to the

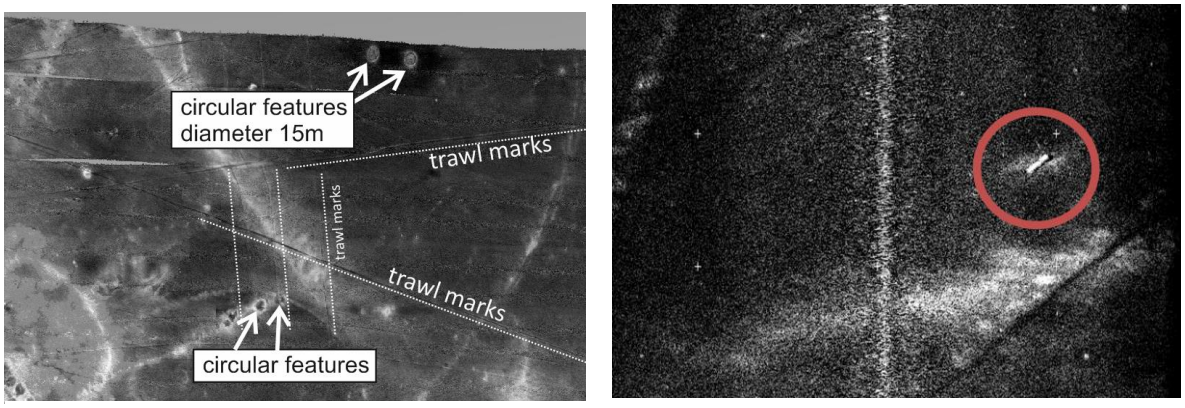

Figure 38: Sidescan data recorded with 300kHz EM2040c and reprocessed. Left: 300kHz Sidescan data re-processed in GEOCODER™ showing remnants of anthropogenic seabed interactions, e.g. trawling marks and circular features from previous explosive mine removal and bubble curtain protections. Right: Red circle highlights a feature potentially representing military equipment.

sidescan and are presented as a slope gradient illuminated 0.8 x 0.8 m grid in Figure 39. The area is characterized by bathymetric highs in the southwest and east. Angular range analyses of the backscatter data (not shown) indicates coarse to medium sand for the highs and fine sand elsewhere which agrees with grab sample sediment classification. Further Figure 39 exposes four sediment wave like features. The northerly elongated feature is approximately 650 m long, 90 m wide, and up to 4 m tall. It remains to be investigated if these features represent potentially moving sand waves or rather stationary outcropping Pleistocene morainic till.

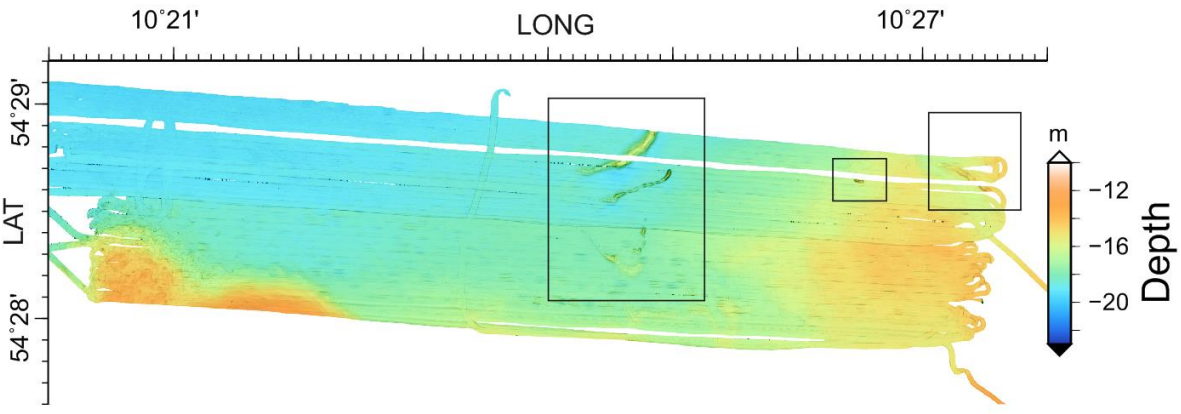

Figure 39: Depth colored bathymetric grid with illumination shaded by slope. Data was recorded with 300kHz EM2040c during AL447. Rectangles indicate potential sand wave locations. Data not yet corrected for water-level fluctuations.

References

Bange, H., Bergmann, K., Hansen, H. P., Kock, A., Koppe, R., Malien, F., & Ostrau, C. (2010). Dissolved methane during hypoxic events at the Boknis Eck time series station (Eckernförde Bay, SW Baltic Sea). *Biogeosciences* (BG), 7, 1279-1284.

Berndt, C., Feseker, T., Treude, T., Krastel, S., Liebetrau, V., Niemann, H., ... & Steinle, L. (2014). Temporal constraints on hydrate-controlled methane seepage off Svalbard. *Science*, *343*(6168), 284-287.

Ciais, P., Sabine, C., Bala, G., Bopp, L., Brovkin, V., Canadell, J., ... & Thornton, P. (2014). Carbon and other biogeochemical cycles. In *Climate Change 2013: The Physical Science Basis. Contribution of Working Group I to the Fifth Assessment Report of the Intergovernmental Panel on Climate Change* (pp. 465-570). Cambridge University Press.

Clift, R., Grace, J. R., & Weber, M. E. (2005). *Bubbles, drops, and particles*. Courier Corporation.

Etiope, G., & Klusman, R. W. (2002). Geologic emissions of methane to the atmosphere. *Chemosphere*, *49*(8), 777-789.

Greinert, J. (2008). Monitoring temporal variability of bubble release at seeps: The hydroacoustic swath system GasQuant. *Journal of Geophysical Research: Oceans (1978–2012)*, *113*(C7)

Holt, J., & Umlauf, L. (2008). Modelling the tidal mixing fronts and seasonal stratification of the Northwest European Continental shelf. *Continental Shelf Research*, *28*(7), 887-903.

Hovland, M., & Sommerville, J. H. (1985). Characteristics of two natural gas seepages in the North Sea. *Marine and Petroleum Geology*, *2*(4), 319-326.

Jackson, D. R., Williams, K. L., Wever, T. F., Friedrichs, C. T., & Wright, L. D. (1998). Sonar evidence for methane ebullition in Eckernförde Bay. *Continental Shelf Research*, *18*(14), 1893-1915.

Jensen, P., I. Aagaard, R. A. Burke, P. R. Dando, N. Joergensen, A. Kuijpers, T. Laier, and R. O'Hara, S.C.M. Schmaljohann (1992). "Bubbling reefs" in the Kattegat: Submarine landscapes of carbonate-cemented rocks support a diverse ecosystem at methane seeps., *Marine Ecology Progress Series*, 83, 103-112.

Judd, A., Davies, G., Wilson, J., Holmes, R., Baron, G., & Bryden, I. (1997). Contributions to atmospheric methane by natural seepages on the UK continental shelf. *Marine Geology*, 137(1), 165-189.

Judd, A. G. (2001). Pockmarks in the UK sector of the North Sea. *UK Department of Trade and Industry Strategic Environmental Assessment Technical Report*.

Judd, A., & Hovland, M. (2007). Seabed fluid flow: the impact on geology, biology and the marine environment. *Cambridge University Press*

Kvenvolden, K. A., Lorenson, T. D., & Reeburgh, W. S. (2001). Attention turns to naturally occurring methane seepage. Eos, *Transactions American Geophysical Union*, 82(40), 457-457.

Niemann, H., Elvert, M., Hovland, M., Orcutt, B., Judd, A., Suck, I., ... & Boetius, A. (2005). Methane emission and consumption at a North Sea gas seep (Tommeliten area). *Biogeosciences, 2,* 335-351, doi:10.5194/bg-2-335-2005.

Ostrovsky, I. (2009). Hydroacoustic assessment of fish abundance in the presence of gas bubbles. *Limnology and Oceanography: Methods*, *7*(4), 309-318.

Pernthaler, A., & Pernthaler, J. (2007). Fluorescence in situ hybridization for the identification of environmental microbes. In *Protocols for Nucleic Acid Analysis by Nonradioactive Probes* (pp. 153-164). Humana Press.

Reeburgh, W. S. (2007). Oceanic methane biogeochemistry. *Chemical Reviews*, *107*(2), 486-513.

Rehder, G., Keir, R. S., Suess, E., & Pohlmann, T. (1998). The Multiple Sources and Patterns of Methane in North Sea Waters. *Aquatic Geochemistry*, *4*(3-4), 403-427.

Schlüter, M., Sauter, E. J., Andersen, C. E., Dahlgaard, H., & Dando, P. R. (2004). Spatial distribution and budget for submarine groundwater discharge in Eckernförde Bay (Western Baltic Sea). *Limnology and Oceanography*, *49*(1), 157-167.

Schmale, O., Schneider von Deimling, J., Gülzow, W., Nausch, G., Waniek, J. J., & Rehder, G. (2010). Distribution of methane in the water column of the Baltic Sea. *Geophysical Research Letters*, 37(12).

Schneider von Deimling (2009), Hydroacoustic and geochemical traces of marine gas seepage in the North Sea, PhD, University Kiel

Schneider von Deimling, J., Greinert, J., Chapman, N. R., Rabbel, W., & Linke, P. (2010). Acoustic imaging of natural gas seepage in the North Sea: Sensing bubbles controlled by variable currents. *Limnology and Oceanography: Methods*, *8*(5), 155-171.

Schneider von Deimling, J., Rehder, G., Greinert, J., McGinnnis, D. F., Boetius, A., & Linke, P. (2011). Quantification of seep-related methane gas emissions at Tommeliten, North Sea. *Continental Shelf Research*, *31*(7), 867-878.

Schneider von Deimling, J. & Papenberg, C. (2012). Detection of gas bubble leakage via correlation of water column multibeam images. *Ocean Science*, 8(2), 175-181.

Schneider von Deimling, J. S., & Weinrebe, W. (2014). Beyond Bathymetry: Water Column Imaging with Multibeam Echo Sounder Systems.

Schroot, B. M., Klaver, G. T., & Schüttenhelm, R. T. (2005). Surface and subsurface expressions of gas seepage to the seabed—examples from the Southern North Sea. *Marine and Petroleum Geology*, *22*(4), 499-515.

Turrell, W. R., Henderson, E. W., Slesser, G., Payne, R., & Adams, R. D. (1992). Seasonal changes in the circulation of the northern North Sea. *Continental Shelf Research*, *12*(2), 257-286.

Wever, T. F., Abegg, F., Fiedler, H. M., Fechner, G., & Stender, I. H. (1998). Shallow gas in the muddy sediments of Eckernförde Bay, Germany. *Continental Shelf Research*, 18(14), 1715-1739.

Wever, T. F., Lühder, R., Voβ, H., & Knispel, U. (2006). Potential environmental control of free shallow gas in the seafloor of Eckernförde Bay, Germany. *Marine geology*, 225(1), 1-4.

Whiticar, M. J., & Werner, F. (1981). Pockmarks: Submarine vents of natural gas or freshwater seeps?. *Geo-Marine Letters*, *1*(3-4), 193-199

Wiesenburg, D. A., & Guinasso Jr, N. L. (1979). Equilibrium solubilities of methane, carbon monoxide, and hydrogen in water and sea water. *Journal of Chemical and Engineering Data*, *24*(4), 356-360.

Wunderlich, J., Müller, S., 2003. High-resolution sub-bottom profiling using parametric acoustics. *International Ocean Systems 7*, 6–11.

Acknowledgements

We would like to express our gratitude for the excellent support by Captain Jan Lass and crew provided during this cruise with R/V ALKOR. Especially the professional maneuvering of a medium sized research vessel like R/V ALKOR in very shallow water requires high navigational skills to allow for precise bathymetric surveying performed throughout the cruise. The technic and logistic center (TLZ), especially the support by Eduard Fabrizius, Kevin Köser, and Matthias Wieck, at GEOMAR, is acknowledged for their excellent support. The cruise has received funding from GEOMAR, the Helmholtz-Alliance the ECO2 project in the European Community's Seventh Framework Program (FP7/2007-2013) under grant agreement n°265847, from the joint European SUGAR II A/BMBF project grant n°03G0819A , as well as from the Future Ocean Project GQ2 (CP1207).

List of Stations

Table 6 Station List AL447

Abbreviation	Full
Ki-Fj	Kiel Fjord
HK	Heidkate
MG	Mittelgrund
MG (E)	Mittelgrund (East)
EF	Eckernförde
LS	Læsø
CTD/RO	CTD/rosette water sampler
MB	Multibeam
CAL	Calibration
PROF	Profile
OFOS	Ocean Floor Observ. System
FI	Flare imaging
CAMS	Calibration Motion Sensor
EL	Elevator Lander
GQ	GasQuant II
SES 2000	SES 2000
PICARRO	Picarro Profil

Date	Time	Station	Gear	Action	Comment	Location	Position Lat	Position Lon
2014/10/20	09:00:00	1320-1	CTD/RO	surface	File: Al227-1 18,8 (Btl. 1; Sound velocity: 1489) 15 (Btl. 2) 10 (Btl. 3) 5 (Btl. 4) 0 (Btl. 5; Sound velocity: 1488-1490) 19,7 PSU salinity Adidtional annotations in the manual station protocol!	Ki-Fj	54° 19,22' N	10° 8,69' E
2014/10/20	09:22:59	1320-1	CTD/RO	on deck		Ki-Fj	54° 19,21' N	10° 8,72' E
2014/10/20	09:23:00	1320-3	MB		MB down to water (vertical shaft)	Ki-Fj	54° 19,22' N	10° 8,69' E
2014/10/20	10:16:00	1320-2	CAL	surface	SB calibration Adidtional annotations in the manual station protocol!	Ki-Fj	54° 19,24' N	10° 8,74' E
2014/10/20	10:19:00	1320-2	CAL	start		Ki-Fj	54° 19,25' N	10° 8,75' E
2014/10/20	15:12:00	1320-2	CAL	End		Ki-Fj	54° 19,20' N	10° 8,70' E
2014/10/20	15:12:59	1320-2	CAL	on deck		Ki-Fj	54° 19,20' N	10° 8,70' E
2014/10/20	16:20:00	1321-1	CAL	start	F180 calibration	Ki-Fj	54° 24,77' N	10° 12,71' E
2014/10/20	18:02:59	1321-1	CAL	End		Ki-Fj	54° 26,01' N	10° 11,89' E

2014/10/20	18:42:00	1322-1	CTD/RO	surface	Sound velocity Lighthouse/wastewater treatment plant	HK	54° 28,56' N	10° 14,39' E
2014/10/20	18:47:59	1322-1	CTD/RO	on deck		HK	54° 28,53' N	10° 14,40' E
2014/10/20	19:02:00	1323-1	CAL	start	MB calibration Partial WCI log for fish-mines-discrimination Appr. 21:00 → munitions Line 11 & 13 → roll calibration	HK	54° 29,42' N	10° 13,92' E
2014/10/20	20:37:59	1323-1	CAL	End		HK	54° 29,51' N	10° 14,20' E
2014/10/20	21:19:00	1324-1	PROF		MB-WCI	HK	54° 28,83' N	10° 20,04' E
2014/10/21	06:34:00	1324-1	PROF		MB-WCI	HK	54° 28,46' N	10° 27,25' E
2014/10/21	06:43:00	1324-2	CTD/RO	surface	Eckernförde-Bay	MG	54° 28,43' N	10° 27,31' E
2014/10/21	06:48:59	1324-2	CTD/RO	on deck		MG	54° 28,42' N	10° 27,29' E
2014/10/21	06:57:00	1324-1	PROF		MB-WCI Eckernförde-Bay	MG	54° 28,46' N	10° 27,28' E
2014/10/21	10:28:00	1324-1	PROF		MB-WCI Eckernförde-Bay	MG	54° 28,37' N	10° 27,21' E
2014/10/21	10:42:00	1325-1	CTD/RO	surface		MG	54° 28,39' N	10° 27,27' E
2014/10/21	10:47:59	1325-1	CTD/RO	on deck		MG	54° 28,39' N	10° 27,28' E
2014/10/21	10:54:00	1324-1	PROF		MB-WCI Eckernförde-Bay	MG	54° 28,35' N	10° 27,21' E
2014/10/21	12:38:00	1324-1	PROF		MB-WCI Eckernförde-Bay	MG	54° 28,32' N	10° 27,26' E
2014/10/21	12:59:00	1324-1	PROF		MB-WCI Eckernförde-Bay	MG	54° 28,77' N	10° 25,26' E
2014/10/21	13:05:00	1324-1	PROF		MB-WCI Eckernförde-Bay	MG	54° 28,34' N	10° 25,19' E
2014/10/21	13:21:00	1324-1	PROF		MB-WCI Eckernförde-Bay	MG	54° 28,44' N	10° 23,02' E
2014/10/21	13:25:00	1324-1	PROF		MB-WCI Eckernförde-Bay	MG	54° 28,77' N	10° 23,03' E
2014/10/21	13:44:00	1324-1	PROF		MB-WCI Eckernförde-Bay	MG	54° 28,94' N	10° 20,74' E
2014/10/21	18:00:59	1324-1	PROF		MB-WCI Eckernförde-Bay	MG	54° 28,60' N	10° 20,21' E
2014/10/21	20:32:00	1326-1	PROF		MB-WCI 4 Eckernförde-Bay	MG	54° 29,69' N	10° 2,56' E
2014/10/21	23:24:00	1326-1	PROF		MB-WCI 4 Eckernförde-Bay	MG	54° 29,81' N	10° 0,65' E
2014/10/21	23:27:00	1327-1	CTD/RO	surface	Eckernförde Bay	MG	54° 29,79' N	10° 0,58' E
2014/10/21	23:32:59	1327-1	CTD/RO	on deck		MG	54° 29,77' N	10° 0,59' E
2014/10/21	23:39:00	1326-1	PROF		MB-WCI	MG	54° 29,84' N	10° 0,54' E
2014/10/22	03:03:59	1326-1	PROF		MB-WCI	MG	54° 30,00' N	10° 0,80' E
2014/10/22	03:30:00	1328-1	PROF		MB-WCI (coninued) additional annotations in manual station protocol 1327-1: Approx. 06:00 → stationary flare imaging on pockmarks	MG	54° 30,01' N	10° 0,64' E
2014/10/22	04:53:59	1328-1	PROF		MB-WCI (continued)	MG	54° 29,94' N	10° 2,40' E
2014/10/22	07:06:00	1329-1	OFOS	surface		MG	54° 29,87' N	10° 1,22' E
2014/10/22	07:15:00	1329-1	OFOS	on deck	OFOS check (07:18 → 1m voreil) Density target, with particles	MG	54° 29,88' N	10° 1,20' E
2014/10/22	07:17:00	1329-1	OFOS	surface		MG	54° 29,87' N	10° 1,20' E
2014/10/22	07:37:00	1329-1	OFOS	on deck		MG	54° 29,87' N	10° 1,20' E
2014/10/22	07:39:00	1329-1	OFOS	surface		MG	54° 29,86' N	10° 1,19' E
2014/10/22	07:58:59	1329-1	OFOS	on deck		MG	54° 29,88' N	10° 1,18' E
2014/10/22	10:01:00	1330-1	CTD/RO	surface	23 (Btl. 1) – 20 – 15 – 10 – 5 – 0 Close to Eckernförde (Pockmarks) With MB-WCI	MG	54° 29,82' N	9° 59,99' E
2014/10/22	10:09:59	1330-1	CTD/RO	on deck		MG	54° 29,82' N	10° 0,00' E

2014/10/22	10:37:00	1331-1	CTD/RO	surface	22 – 20 – 15 – 10 – 5 – 0 Close to Eckernförde (Pockmarks) With MB-WCI	MG	54° 29,85' N	10° 0,61' E
2014/10/22	10:44:59	1331-1	CTD/RO	on deck		MG	54° 29,85' N	10° 0,61' E
2014/10/22	10:57:00	1332-1	CTD/RO	surface	1 – 5 – 10 – 15 – 20 – 24 Close to Eckernförde (Pockmarks) With MB-WCI	MG	54° 29,87' N	10° 1,19' E
2014/10/22	11:05:59	1332-1	CTD/RO	on deck		MG	54° 29,87' N	10° 1,22' E
2014/10/22	11:48:00	1333-1	CTD/RO	surface	1 – 5 – 10 – 15 – 20 – 23 Close to Eckernförde (Pockmarks) With MB-WCI	MG	54° 29,89' N	10° 1,85' E
2014/10/22	11:55:59	1333-1	CTD/RO	on deck		MG	54° 29,89' N	10° 1,87' E
2014/10/22	12:08:00	1334-1	CTD/RO	surface	1 – 5 – 10 – 15 – 20 – 22 Close to Eckernförde (Pockmarks) With MB-WCI	MG	54° 29,93' N	10° 2,40' E
2014/10/22	12:14:59	1334-1	CTD/RO	on deck		MG	54° 29,93' N	10° 2,40' E
2014/10/22	12:36:00	1335-1	CTD/RO	surface	1 – 5 – 10 – 15 – 20 – 22 Close to Eckernförde (Pockmarks) With MB-WCI	MG	54° 30,44' N	10° 1,47' E
2014/10/22	12:42:59	1335-1	CTD/RO	on deck		MG	54° 30,42' N	10° 1,42' E
2014/10/22	13:02:00	1336-1	CTD/RO	surface	1 – 5 – 10 – 15 – 20 – 23 Close to Eckernförde (Pockmarks) With MB-WCI	MG	54° 30,12' N	10° 1,30' E
2014/10/22	13:07:59	1336-1	CTD/RO	on deck		MG	54° 30,13' N	10° 1,31' E
2014/10/22	13:08:00	1337-1	CTD/RO	surface	1 – 5 – 10 – 15 – 20 – 22 Close to Eckernförde (Pockmarks) With MB-WCI	MG	54° 30,13' N	10° 1,32' E
2014/10/22	13:26:59	1337-1	CTD/RO	on deck		MG	54° 29,61' N	10° 1,11' E
2014/10/22	13:38:00	1338-1	CTD/RO	surface	1 – 5 – 10 – 15 – 20 – 22 Close to Eckernförde (Pockmarks) With MB-WCI	MG	54° 29,31' N	10° 0,99' E
2014/10/22	13:44:59	1338-1	CTD/RO	on deck		MG	54° 29,32' N	10° 1,00' E
2014/10/22	14:24:00	1339-1	FI		MB-WCI, EK60 Pockmarks	MG	54° 29,88' N	10° 1,22' E
2014/10/22	16:25:59	1339-1	FI		MB-WCI, EK60 Pockmarks	MG	54° 29,80' N	10° 1,21' E
2014/10/22	16:30:00	1340-1	CAMS		F180 calibration	MG	54° 29,88' N	10° 1,21' E
2014/10/22	17:41:59	1340-1	CAMS		F180 calibration	MG	54° 29,78' N	10° 1,32' E
2014/10/22	18:02:00	1341-1	PROF		SBP	MG	54° 29,93' N	10° 0,64' E
2014/10/22	19:45:59	1341-1	PROF		SBP	MG	54° 30,23' N	10° 1,67' E
2014/10/22	20:03:00	1342-1	FI		MB WCI Bubbles!	MG	54° 29,83' N	10° 1,24' E
2014/10/23	03:01:59	1342-1	FI		MB WCI Bubbles!	MG	54° 29,67' N	10° 1,26' E
2014/10/23	03:19:00	1343-1	CTD/RO	surface	1 – 5 – 10 – 15 – 20 – 23 Close to Eckernförde	MG	54° 29,82' N	10° 0,03' E
2014/10/23	03:27:59	1343-1	CTD/RO	on deck		MG	54° 29,82' N	9° 59,99' E
2014/10/23	03:55:00	1344-1	CTD/RO	surface	1 – 5 – 10 – 15 – 20 – 23 Close to Eckernförde	MG	54° 29,84' N	10° 0,61' E
2014/10/23	04:01:59	1344-1	CTD/RO	on deck		MG	54° 29,86' N	10° 0,61' E
2014/10/23	04:18:00	1345-1	CTD/RO	surface	1 – 5 – 10 – 15 – 20 – 24 Close to Eckernförde Bubble streams on EK60	MG	54° 29,86' N	10° 1,20' E
2014/10/23	04:24:59	1345-1	CTD/RO	on deck		MG	54° 29,88' N	10° 1,20' E
2014/10/23	05:21:00	1346-1	CTD/RO	surface	1 – 5 – 10 – 15 – 20 – 24 Close to Eckernförde	MG	54° 29,90' N	10° 1,84' E
2014/10/23	05:28:59	1346-1	CTD/RO	on deck		MG	54° 29,89' N	10° 1,82' E
2014/10/23	05:44:00	1347-1	CTD/RO	surface	1 – 5 – 10 – 15 – 20 – 22 Close to Eckernförde	MG	54° 29,93' N	10° 2,39' E
2014/10/23	05:49:59	1347-1	CTD/RO	on deck		MG	54° 29,96' N	10° 2,37' E
2014/10/23	06:13:00	1348-1	CTD/RO	surface	1 – 5 – 10 – 15 – 20 – 23 Close to Eckernförde	MG	54° 30,48' N	10° 1,43' E
2014/10/23	06:19:59	1348-1	CTD/RO	on deck		MG	54° 30,44' N	10° 1,44' E

2014/10/23	06:40:00	1349-1	CTD/RO	surface	1 – 5 – 10 – 15 – 20 – 23 Close to Eckernförde	MG	54° 30,15' N	10° 1,34' E
2014/10/23	06:46:59	1349-1	CTD/RO	on deck		MG	54° 30,15' N	10° 1,34' E
2014/10/23	07:03:00	1350-1	CTD/RO	surface	1 – 5 – 10 – 15 – 20 – 22 Close to Eckernförde	MG	54° 29,62' N	10° 1,10' E
2014/10/23	07:09:59	1350-1	CTD/RO	on deck		MG	54° 29,57' N	10° 1,10' E
2014/10/23	07:19:00	1351-1	CTD/RO	surface	1 – 5 – 10 – 15 – 20 – 22 Close to Eckernförde	MG	54° 29,31' N	10° 1,03' E
2014/10/23	07:24:59	1351-1	CTD/RO	on deck		MG	54° 29,31' N	10° 1,04' E
2014/10/23	07:33:59	1320-3	MB		MB out of vertical shaft	HK	54° 29,33' N	10° 1,45' E
2014/10/23	17:45:00	1352-1	MB		MB down to water (vertical shaft)	HK	54° 28,58' N	10° 20,44' E
2014/10/23	17:48:00	1352-2	CTD/RO	surface	Sound velocity, max. depth: 15m	HK	54° 28,56' N	10° 20,45' E
2014/10/23	17:52:59	1352-2	CTD/RO	on deck		HK	54° 28,55' N	10° 20,44' E
2014/10/23	17:58:00	1353-1	CAMS		1st F180 calibration	HK	54° 28,53' N	10° 20,47' E
2014/10/23	18:19:59	1353-1	CAMS			HK	54° 28,52' N	10° 20,82' E
2014/10/23	18:29:00	1354-1	PROF		MB mapping File: heidkate3	HK	54° 28,55' N	10° 20,70' E
2014/10/23	20:32:00	1354-1	PROF		MB mapping	HK	54° 28,46' N	10° 22,13' E
2014/10/23	21:34:00	1354-1	PROF		MB mapping	HK	54° 28,51' N	10° 20,56' E
2014/10/24	04:20:59	1354-1	PROF		MB mapping	HK	54° 28,36' N	10° 20,79' E
2014/10/24	06:19:00	1355-1	EL		Elevator swim-check	MG	54° 29,89' N	10° 1,21' E
2014/10/24	06:21:00	1355-1	EL			MG	54° 29,89' N	10° 1,22' E
2014/10/24	07:32:00	1355-1	EL			MG	54° 30,04' N	10° 0,61' E
2014/10/24	07:48:59	1355-1	EL		Elevator Deployment	MG	54° 30,05' N	10° 0,61' E
2014/10/24	07:55:00	1356-1	FI		EK60 57ml/min	MG	54° 30,08' N	10° 0,61' E
2014/10/24	10:55:59	1356-1	FI		EK60	MG	54° 30,00' N	10° 0,54' E
2014/10/24	11:59:59	1357-1	EL		Elevator recovery (additional annotations for station 1369-1 in the Manual station protocol!)	MG	54° 30,06' N	10° 0,65' E
2014/10/24	13:00:00	1358-1	GQ		Drop-down GQ	MG	54° 29,89' N	10° 1,22' E
2014/10/24	13:01:59	1358-1	GQ			MG	54° 29,88' N	10° 1,22' E
2014/10/24	13:31:00	1359-1	CTD/RO	surface	1 – 5 – 10 – 15 - 20 – 22 Close to Eckernförde	MG	54° 29,82' N	10° 0,06' E
2014/10/24	13:36:59	1359-1	CTD/RO	on deck		MG	54° 29,81' N	10° 0,07' E
2014/10/24	13:57:00	1360-1	CTD/RO	surface	1 – 5 – 10 – 15 - 20 – 22 Close to Eckernförde	MG	54° 29,85' N	10° 0,59' E
2014/10/24	14:02:59	1360-1	CTD/RO	on deck		MG	54° 29,86' N	10° 0,61' E
2014/10/24	14:36:00	1361-1	CTD/RO	surface	1 – 5 – 10 – 15 - 20 – 24 Close to Eckernförde	MG	54° 29,90' N	10° 1,56' E
2014/10/24	14:41:59	1361-1	CTD/RO	on deck		MG	54° 29,89' N	10° 1,55' E
2014/10/24	15:01:00	1362-1	CTD/RO	surface	1 – 5 – 10 – 15 - 20 – 23 Close to Eckernförde	MG	54° 29,90' N	10° 1,86' E
2014/10/24	15:06:59	1362-1	CTD/RO	on deck		MG	54° 29,91' N	10° 1,86' E
2014/10/24	15:24:00	1363-1	CTD/RO	surface	1 – 5 – 10 – 15 - 20 – 22 Close to Eckernförde	MG	54° 29,94' N	10° 2,46' E
2014/10/24	15:30:59	1363-1	CTD/RO	on deck		MG	54° 29,94' N	10° 2,44' E
2014/10/24	16:36:00	1364-1	PROF		MB mapping, afterwards WCI flare imaging Annotation: 20:03 → Flare imaging	MG (E)	54° 30,25' N	10° 0,30' E
2014/10/24	20:07:00	1364-1	PROF		MB mapping	MG (E)	54° 29,33' N	9° 58,14' E
2014/10/24	22:25:59	1364-1	PROF		MB mapping	MG (E)	54° 29,82' N	9° 59,08' E
2014/10/24	22:52:00	1365-1	SES 2000		Pockmarks (south of Eckernförde Bay) Shallow gas under different angles	EF	54° 29,02' N	10° 1,73' E
2014/10/25	02:20:59	1365-1	SES 2000			EF	54° 28,67' N	9° 59,78' E
2014/10/25	02:39:00	1366-1	PROF		MB	MG	54° 29,36' N	9° 58,46' E
2014/10/25	04:26:00	1366-1	PROF		MB	MG	54° 29,59' N	10° 0,30' E
2014/10/25	04:56:00	1366-1	PROF		MB	MG	54° 29,96' N	9° 58,42' E
2014/10/25	05:49:59	1366-1	PROF		MB	MG	54° 29,90' N	9° 58,10' E

2014/10/25	06:13:00	1367-1	CTD/RO	surface	1 – 5 – 10 – 15 – 20 – 23 Close to Eckernförde	MG	54° 29,89' N	10° 1,40' E
2014/10/25	06:18:59	1367-1	CTD/RO	on deck		MG	54° 29,86' N	10° 1,42' E
2014/10/25	06:21:00	1368-1	FI		Drift	MG	54° 29,85' N	10° 1,43' E
2014/10/25	09:55:59	1368-1	FI		Drift	MG	54° 29,83' N	10° 1,32' E
2014/10/25	10:14:00	1369-1	OFOS	surface	10:22 → OFOS track begins (track in the east of the GQ) Annotations from manual station protocol 1357-1: 10:43 → Flares/Bubbles 10:51 → Bubbles in video! 1st track: 15m shackle depth 2nd track: 21m shackle depth 3rd track: 20m shackle depth	MG	54° 30,04' N	10° 1,39' E
2014/10/25	10:53:59	1369-1	OFOS	on deck		MG	54° 29,78' N	10° 1,26' E
2014/10/25	11:05:00	1369-2	OFOS	surface	Annotations from manual station protocol 1357-1: 11:08 → OFOS to water	MG	54° 30,02' N	10° 1,35' E
2014/10/25	11:50:59	1369-2	OFOS	on deck	Annotations from manual station protocol 1357-1: 11:35 → Bubbles/Flares	MG	54° 29,83' N	10° 1,30' E
2014/10/25	12:08:00	1369-3	OFOS	surface		MG	54° 29,96' N	10° 1,38' E
2014/10/25	12:56:59	1369-3	OFOS	on deck		MG	54° 29,83' N	10° 1,31' E
2014/10/25	13:33:59	1370-1	GQ		Pick up-procedure	MG	54° 29,88' N	10° 1,21' E
2014/10/25	14:12:00	1371-1	PROF		MB, ADCP during turns	MG	54° 30,03' N	9° 59,20' E
2014/10/25	14:22:00	1371-1	PROF		MB, ADCP during turns	MG	54° 29,61' N	9° 59,21' E
2014/10/25	14:26:00	1371-1	PROF		MB, ADCP during turns	MG	54° 29,64' N	9° 59,16' E
2014/10/25	16:32:59	1371-1	PROF		MB, ADCP during turns	MG	54° 29,44' N	9° 57,56' E
2014/10/25	18:59:00	1372-1	MB		MB calibration pitch & yaw	MG	54° 30,10' N	10° 1,40' E
2014/10/25	20:08:59	1372-1	MB		MB calibration pitch & yaw	MG	54° 29,41' N	10° 1,44' E
2014/10/25	22:10:00	1373-1	MB		MB calibration pitch & yaw	HK	54° 28,37' N	10° 20,52' E
2014/10/26	07:33:59	1373-1	MB		MB calibration pitch & yaw	HK	54° 27,99' N	10° 27,23' E
2014/10/26	07:42:00	1374-1	CTD/RO	surface	Sound velocity	HK	54° 27,99' N	10° 27,16' E
2014/10/26	07:46:59	1374-1	CTD/RO	on deck		HK	54° 27,99' N	10° 27,17' E
2014/10/26	08:28:00	1375-1	CTD/RO	surface	1 – 5 – 10 – 15 – 17,5 Referece for Eckernförde-Bay	HK	54° 29,06' N	10° 23,66' E
2014/10/26	08:32:59	1375-1	CTD/RO	on deck		HK	54° 29,04' N	10° 23,67' E
2014/10/26	08:37:59	1352-1	MB		MB out of vertical shaft	LS	54° 29,03' N	10° 23,63' E
2014/10/27	01:54:00	1376-1	MB		MB down to water (vertical shaft)	LS	57° 18,76' N	10° 39,11' E
2014/10/27	02:05:00	1377-1	PROF		SBP	LS	57° 19,54' N	10° 38,65' E
2014/10/27	09:59:59	1377-1	PROF		SBP	LS	57° 26,38' N	10° 55,13' E
2014/10/27	10:14:00	1378-1	CTD/RO	surface	Sound velocity	LS	57° 26,41' N	10° 54,83' E
2014/10/27	10:20:59	1378-1	CTD/RO	on deck		LS	57° 26,36' N	10° 54,81' E
2014/10/27	10:44:00	1379-1	PROF		MB-WCI	LS	57° 26,99' N	10° 57,93' E
2014/10/27	14:29:59	1379-1	PROF		MB-WCI	LS	57° 26,97' N	10° 58,10' E
2014/10/27	14:31:59	1376-1	MB		MB out of vertical shaft	LS	57° 26,96' N	10° 57,95' E
2014/10/28	09:21:00	1380-1	MB		MB down to water (vertical shaft)	LS	57° 26,91' N	10° 42,62' E
2014/10/28	09:24:00	1381-1	PICARRO			LS	57° 26,99' N	10° 42,97' E
2014/10/28	12:31:59	1381-1	PICARRO			LS	57° 32,00' N	11° 10,00' E
2014/10/28	13:54:00	1382-1	PROF		MB-WCI	LS	57° 26,97' N	11° 10,08' E
2014/10/28	18:08:59	1382-1	PROF		MB-WCI	LS	57° 26,88' N	10° 58,32' E
2014/10/28	18:16:00	1383-1	FI			LS	57° 26,63' N	10° 57,30' E
2014/10/28	19:12:59	1383-1	FI			LS	57° 25,95' N	10° 55,61' E
2014/10/28	19:35:00	1384-1	CTD/RO	surface	1 – 5 – 10 – 15 – 18	LS	57° 26,33' N	10° 56,47' E
2014/10/28	19:42:59	1384-1	CTD/RO	on deck		LS	57° 26,32' N	10° 56,49' E
2014/10/28	21:50:00	1385-1	CTD/RO	surface		LS	57° 25,95' N	10° 57,85' E
2014/10/28	21:55:59	1385-1	CTD/RO	on deck		LS	57° 25,94' N	10° 57,84' E
2014/10/28	22:30:00	1386-1	CTD/RO	surface	1 – 5 – 10 – 15 – 17 Dirty weather	LS	57° 26,31' N	10° 56,52' E
2014/10/28	22:36:59	1386-1	CTD/RO	on deck		LS	57° 26,32' N	10° 56,52' E
2014/10/28	23:16:00	1387-1	FI			LS	57° 26,51' N	10° 57,14' E

2014/10/29	07:31:59	1387-1	FI			LS	57° 26,45' N	10° 58,09' E
2014/10/29	11:51:00	1388-1	FI			LS	57° 25,73' N	10° 55,94' E
2014/10/29	13:51:59	1388-1	FI			LS	57° 26,82' N	11° 0,03' E
2014/10/29	14:18:00	1389-1	CTD/RO	surface	1 – 5 – 8	LS	57° 25,54' N	10° 58,79' E
2014/10/29	14:23:59	1389-1	CTD/RO	on deck		LS	57° 25,53' N	10° 58,77' E
2014/10/29	14:44:00	1390-1	CTD/RO	surface	1 – 5 – 10 -13	LS	57° 26,48' N	10° 58,78' E
2014/10/29	14:48:59	1390-1	CTD/RO	on deck		LS	57° 26,50' N	10° 58,79' E
2014/10/29	15:09:00	1391-1	CTD/RO	surface	1 – 5 – 10 – 14	LS	57° 26,00' N	10° 56,50' E
2014/10/29	15:13:59	1391-1	CTD/RO	on deck		LS	57° 26,00' N	10° 56,46' E
2014/10/29	15:27:00	1392-1	FI			LS	57° 25,59' N	10° 55,71' E
2014/10/30	05:53:59	1392-1	FI			LS	57° 26,21' N	10° 59,18' E
2014/10/30	06:56:00	1393-1	CTD/RO	surface	Sound velocity	LS	57° 26,29' N	10° 56,52' E
2014/10/30	07:00:59	1393-1	CTD/RO	on deck		LS	57° 26,30' N	10° 56,54' E
2014/10/30	07:20:00	1394-1	OFOS	surface	Bbox towtrack Rope length: 12m, shackle surface This means: Bbox approx. 14m Check MB WCI	LS	57° 26,29' N	10° 56,54' E
2014/10/30	09:45:59	1394-1	OFOS	on deck		LS	57° 26,31' N	10° 56,51' E
2014/10/30	09:48:00	1395-1	FI			LS	57° 26,30' N	10° 56,51' E
2014/10/30	11:02:59	1395-1	FI			LS	57° 26,26' N	10° 56,79' E
2014/10/30	11:09:00	1396-1	OFOS	surface	Track 1	LS	57° 26,30' N	10° 56,68' E
2014/10/30	11:48:59	1396-1	OFOS	on deck		LS	57° 26,29' N	10° 56,45' E
2014/10/30	11:59:00	1396-2	OFOS	surface	Track 2	LS	57° 26,29' N	10° 56,71' E
2014/10/30	12:33:59	1396-2	OFOS	on deck		LS	57° 26,30' N	10° 56,43' E
2014/10/30	12:46:00	1396-3	OFOS	surface	Track 3	LS	57° 26,28' N	10° 56,68' E
2014/10/30	13:12:59	1396-3	OFOS	on deck		LS	57° 26,27' N	10° 56,49' E
2014/10/30	13:25:00	1397-1	GQ			LS	57° 26,27' N	10° 56,53' E
2014/10/30	13:26:00	1397-1	GQ			LS	57° 26,27' N	10° 56,53' E
2014/10/30	13:28:59	1397-1	GQ			LS	57° 26,27' N	10° 56,53' E
2014/10/30	14:01:00	1398-1	CTD/RO	surface	1 – 5 – 10 – 15 – 17 (with gas flares → total-gas-analytic-probes)	LS	57° 26,31' N	10° 56,53' E
2014/10/30	14:11:59	1398-1	CTD/RO	on deck		LS	57° 26,29' N	10° 56,56' E
2014/10/30	14:28:00	1399-1	CTD/RO	surface	1 – 5 – 10 – 15 – 17	LS	57° 26,31' N	10° 56,57' E
2014/10/30	14:32:59	1399-1	CTD/RO	on deck		LS	57° 26,31' N	10° 56,56' E
2014/10/30	14:51:00	1400-1	CTD/RO	surface	1 – 5 – 10 – 15 – 18	LS	57° 26,30' N	10° 56,49' E
2014/10/30	14:54:59	1400-1	CTD/RO	on deck		LS	57° 26,30' N	10° 56,49' E
2014/10/30	15:11:00	1401-1	FI		EK-60	LS	57° 26,06' N	10° 57,85' E
2014/10/30	23:30:59	1401-1	FI		EK-60	LS	57° 26,05' N	10° 57,18' E
2014/10/30	23:44:00	1402-1	SES 2000		Profiles	LS	57° 25,76' N	10° 55,89' E
2014/10/31	03:33:59	1402-1	SES 2000		Profiles	LS	57° 27,10' N	10° 57,40' E
2014/10/31	03:49:00	1403-1	FI		MB-WCI & EK-60	LS	57° 26,87' N	10° 57,90' E
2014/10/31	06:51:59	1403-1	FI		MB-WCI & EK-60	LS	57° 27,04' N	10° 57,37' E
2014/10/31	07:02:00	1404-1	CTD/RO	surface	Sound velocity	LS	57° 27,14' N	10° 57,90' E
2014/10/31	07:08:59	1404-1	CTD/RO	on deck		LS	57° 27,13' N	10° 57,91' E
2014/10/31	07:44:00	1405-1	FI		MB-WCI Continuation of station 1403-1	LS	57° 25,72' N	10° 57,99' E
2014/10/31	10:51:00	1406-1	FI		MB-WCI Gap-filling	LS	57° 25,58' N	10° 57,80' E
2014/10/31	10:51:59	1405-1	FI			LS	57° 25,58' N	10° 57,80' E
2014/10/31	12:59:59	1406-1	FI			LS	57° 25,39' N	10° 56,50' E
2014/10/31	13:26:00	1407-1	GQ		Pick-up procedure 13:26 → Bottom-weight back on deck 13:28 → GQ on deck Kelp with bryozoan (89cm)	LS	57° 26,28' N	10° 56,57' E
2014/10/31	13:28:59	1407-1	GQ			LS	57° 26,28' N	10° 56,56' E
2014/10/31	13:41:00	1408-1	CTD/RO	surface	1 – 5 – 10 – 15 – 17 Picarro peak at CTD	LS	57° 26,31' N	10° 56,53' E
2014/10/31	13:45:59	1408-1	CTD/RO	on deck		LS	57° 26,31' N	10° 56,52' E
2014/10/31	13:58:00	1409-1	SES 2000		across chimney1	LS	57° 25,98' N	10° 55,57' E

2014/10/31	15:00:59	1409-1	SES 2000			LS	57° 26,65' N	10° 56,16' E
2014/10/31	15:03:59	1380-1	MB		MB out of vertical shaft	LS	57° 26,80' N	10° 55,88' E
2014/11/01	12:18:00	1410-1	CTD/RO	surface	1 – 5 – 10 – 15 – 20 – 25 – 27 Additional: ADCP Close to Eckernförde	MG	54° 30,74' N	10° 0,40' E
2014/11/01	12:24:59	1410-1	CTD/RO	on deck		MG	54° 30,74' N	10° 0,43' E
2014/11/01	12:33:00	1411-1	MB		MB down to water (vertical shaft)	MG	54° 30,31' N	10° 0,93' E
2014/11/01	12:51:00	1412-1	CTD/RO	surface	1 – 5 – 10 – 15 – 20 – 23 Additional: ADCP Close to Eckernförde	MG	54° 30,29' N	10° 0,95' E
2014/11/01	12:55:59	1412-1	CTD/RO	on deck		MG	54° 30,31' N	10° 0,93' E
2014/11/01	13:17:00	1413-1	CTD/RO	surface	1 – 5 – 10 – 15 – 20 – 24 (approx.) Additional: ADCP → Flares! Close to Eckernförde	MG	54° 29,89' N	10° 1,24' E
2014/11/01	13:22:59	1413-1	CTD/RO	on deck		MG	54° 29,89' N	10° 1,23' E
2014/11/01	13:29:00	1414-1	GQ		In pockmark; GQ upturned	MG	54° 29,88' N	10° 1,22' E
2014/11/01	13:30:00	1414-1	GQ		GQ to water	MG	54° 29,88' N	10° 1,23' E
2014/11/01	13:32:59	1414-1	GQ		Bottom-weight into water	MG	54° 29,87' N	10° 1,24' E
2014/11/01	13:51:00	1415-1	CTD/RO	surface	1 – 5 – 10 – 15 – 20 – 22 Additional: ADCP Close to Eckernförde	MG	54° 29,50' N	10° 1,51' E
2014/11/01	13:56:59	1415-1	CTD/RO	on deck		MG	54° 29,50' N	10° 1,51' E
2014/11/01	14:11:00	1416-1	CTD/RO	surface	1 – 5 – 10 – 15 – 20 (approx.) Additional: ADCP Close to Eckernförde	MG	54° 29,06' N	10° 1,75' E
2014/11/01	14:16:59	1416-1	CTD/RO	on deck		MG	54° 29,06' N	10° 1,75' E
2014/11/01	14:53:00	1417-1	FI			MG	54° 30,88' N	10° 0,41' E
2014/11/02	03:37:59	1417-1	FI			MG	54° 28,94' N	10° 0,49' E
2014/11/02	04:05:00	1418-1	CTD/RO	surface	1 – 5 – 10 – 15 – 20 – 25 – 27 (approx.) Additional: ADCP → Flares! Close to Eckernförde	MG	54° 30,75' N	10° 0,39' E
2014/11/02	04:10:59	1418-1	CTD/RO	on deck		MG	54° 30,73' N	10° 0,39' E
2014/11/02	04:43:00	1419-1	CTD/RO	surface	1 – 5 – 10 – 15 – 20 – 25 – 23 Additional: ADCP Close to Eckernförde	MG	54° 30,30' N	10° 0,93' E
2014/11/02	04:48:59	1419-1	CTD/RO	on deck		MG	54° 30,29' N	10° 0,91' E
2014/11/02	05:05:00	1420-1	CTD/RO	surface	1 – 5 – 10 – 15 – 20 – 25 – 22 (approx.) Additional: ADCP Close to Eckernförde	MG	54° 29,89' N	10° 1,29' E
2014/11/02	05:10:59	1420-1	CTD/RO	on deck		MG	54° 29,90' N	10° 1,35' E
2014/11/02	05:33:00	1421-1	CTD/RO	surface	1 – 5 – 10 – 15 – 20 – 25 – 21,5 (approx.) Additional: ADCP Close to Eckernförde	MG	54° 29,51' N	10° 1,48' E
2014/11/02	05:37:59	1421-1	CTD/RO	on deck		MG	54° 29,50' N	10° 1,49' E
2014/11/02	05:57:00	1422-1	CTD/RO	surface	1 – 5 – 10 – 15 – 20 Additional: ADCP Close to Eckernförde	MG	54° 29,06' N	10° 1,74' E
2014/11/02	06:02:59	1422-1	CTD/RO	on deck		MG	54° 29,06' N	10° 1,74' E
2014/11/02	06:27:00	1423-1	MB		Profiles Pockmark mapping (south of Mittelgrund)	MG	54° 29,25' N	10° 2,23' E
2014/11/02	07:07:59	1423-1	MB		Profiles Pockmark mapping (south of Mittelgrund)	MG	54° 29,21' N	10° 2,18' E
2014/11/02	07:54:00	1424-1	CAL	start		MG	54° 29,55' N	10° 1,24' E
2014/11/03	05:24:59	1430-1	MB			HK	54° 28,50' N	10° 26,98' E
2014/11/03	06:31:00	1431-1	BG	surface		HK	54° 25,14' N	10° 32,69' E
2014/11/03	06:35:59	1431-1	BG	on deck		HK	54° 25,14' N	10° 32,69' E
2014/11/03	06:54:00	1431-2	BG	surface		HK	54° 25,11' N	10° 32,65' E
2014/11/03	06:55:59	1431-2	BG	on deck		HK	54° 25,10' N	10° 32,67' E

2014/11/03	07:35:00	1432-1	EL		HK	54° 25,10' N	10° 32,65' E
2014/11/03	07:39:59	1432-1	EL		HK	54° 25,10' N	10° 32,65' E
2014/11/03	07:42:00	1433-1	FI		HK	54° 25,11' N	10° 32,66' E
2014/11/03	09:50:59	1433-1	FI		HK	54° 25,10' N	10° 32,67' E
2014/11/03	10:09:00	1434-1	PROF		HK	54° 25,46' N	10° 32,68' E
2014/11/03	10:54:59	1434-1	PROF		HK	54° 25,07' N	10° 32,65' E
2014/11/03	11:09:00	1435-1	EL		HK	54° 25,18' N	10° 32,77' E
2014/11/03	11:17:00	1435-1	EL		HK	54° 25,09' N	10° 32,69' E
2014/11/03	11:20:59	1435-1	EL		HK	54° 25,10' N	10° 32,67' E
2014/11/03	12:16:00	1436-1	CTD/RO	surface	HK	54° 27,75' N	10° 27,31' E
2014/11/03	12:19:59	1436-1	CTD/RO	on deck	HK	54° 27,75' N	10° 27,30' E
2014/11/03	13:22:00	1437-1	FI		HK	54° 28,16' N	10° 20,46' E
2014/11/04	02:55:59	1437-1	FI		HK	54° 29,08' N	10° 19,89' E
2014/11/04	02:58:59	1411-1	MB		HK	54° 28,97' N	10° 19,82' E